SPIS TREŚCI

ZESZYTY NAUKOWE POLITECHNIKI RZESZOWSKIEJ **Nr 284**
Mechanika z. 84 (4/12) **2012**

Paweł FROŃ
REMET S.A., Stalowa Wola
Feliks STACHOWICZ
Rzeszow University of Technology

BENDING FORCE AND SPRINGBACK CHARACTERISTICS OF THE TAILOR-WELDED 18G2A-E355 STEEL STRIPS

In many studies a wide range of information about the bendability, failure patterns and the springback of homogeneous as well as tailor-welded sheet metal parts are presented. However, accurate prediction of the springback remains elusive, especially in the case of thick sheet metal. The purpose of this study was experimental determination of the bending force and springback coefficient of the tailor-welded 18G2A-E355 steel strips. Especially, it was focused on comparing the differences in the mechanical properties and bending characteristics between the tailor-welded strips and non-welded ones under the same experimental conditions. The set-up mounted on the testing machine, instrumentation and process control system allows the rig to operate in displacement as well as load control. The MAG method with the Argon + CO_2 atmosphere was used for strips welding.

Keywords: tailor-welded sheet metal, strain hardening, bending force, springback

1. Introduction

Bending is one of major sheet and strips forming operations widely used in modern industries. For this reason, understanding the bending process helps to provide some information crucial to industrial production. Recently many industry companies are trying to form different products by using tailor-welded blanks. A tailor-welded blank consists of two or more sheets that have been welded together in a single plane prior to forming. And the sheets joined by welding can be identical, or they can have different thickness, mechanical properties or surface coatings. Various welding processes, i.e. laser welding, mash welding, electron-beam welding or induction welding, can join them.

In the field of sheet metal bending, one can find literature on pure bending, V-die bending, simple flanging and so on. Most materials can be bent to quite a small radius, but a problem is to control the shape of the bend workpiece. In general, a bend workpiece will recover elasticity i.e. springback on unloading, so

that the bend quality is heavily dependent on the springback, which is a function of material properties and process parameters such as Young's modulus, yield stress, strain hardening abilities, plastic anisotropy, thickness and die geometry [1-6]. The most important die bending process is bending in a V-shaped die, so that deformed shape results from the sheet being pressed into the die by the punch until it is in contact with the sides of the die to the maximum extent possible.

Springback is a phenomenon in which the metal strip unbends itself after a forming operation. Control of springback for the bending processes applied in practice is difficult for a number of reasons, especially in mass production [2, 7-12]. In the case of tailor-welded strips the quality of the weld is critical for a successful forming operation [13, 14] and affects springback phenomenon [15, 16]. Sheet metal forming processes, such as bending, stretching and drawing are widely applied industrially, but design of tools and selection of sheet material remain almost invariably dependent on trial and error [8]. The main reason is that the shape of tools, characteristics of material, process variables and the geometric configuration of the workpiece all influence the manufacturing process: these characteristics are difficult to formulate into a precise mathematical model. The evaluation of elastic springback effects is a fundamental aspect in the practice of sheet forming operations. Springback, in fact, introduces deviations from the desired final shape – consequently, the stamped sheet does not conform to the design specifications and could result in being unsuitable for the application. A complete knowledge of the springback phenomenon and its dependence on material and process variables is strongly required in order to develop effective real time process control systems.

The main purpose of this study was experimental determination of the bending force and springback coefficient of the tailor-welded 18G2A-E355 steel strips. Especially, it was focused on comparing the differences of the mechanical properties and bending characteristics between the tailor-welded strips and non-welded ones under the same experimental conditions.

2. Experimental materials and methods

The 18G2A-E355 steel strips, 9.0 mm thick were used in this experiment. The MAG method with the Argon + CO_2 atmosphere was used for strips welding. Geometry of strip edge prepared for welding is presented in Fig. 1. When the mechanical testing is concerned, 3 types of tensile specimens (Fig. 2) of 240 mm gauge length and 12.5 mm width in gauge region were prepared from:

- based material strip,
- strip containing longitudinal weld,
- strip containing transverse weld.

The experiments were carried out using a special device, which recorded simultaneously the tensile load, the current length of the specimens.

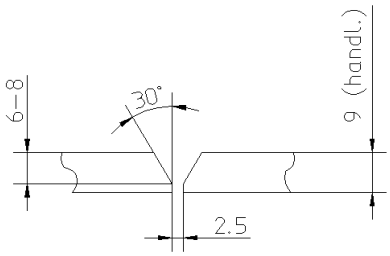

Fig. 1. Geometry of strip edge prepared for welding

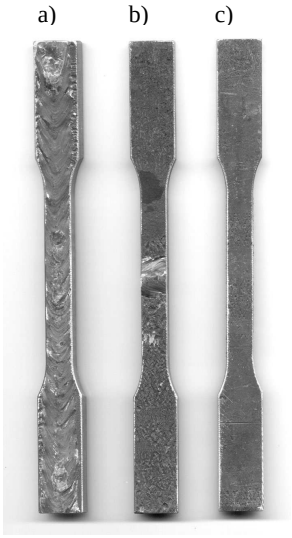

Fig. 2. Tensile specimens – with longitudinal weld (a), transverse weld (b) and base material (c)

For many years strain hardening laws such as those from Ludwig, Hollomon, Voce, Swift and Krupkowski have been used to describe the plastic behaviour of polycrystalline metals and alloys. The Hollomon law in the form of:

$$\sigma = C\varepsilon^n \tag{1}$$

has been used the most frequently. The parameters involved in this law, particularly n-value have been correlated to changes in the microstructure of a material and in some way represent processes, which occur during deformation. They have also been used extensively to characterise the formability of sheet material. The value of strain hardening exponent, n, is usually determined from the double logarithmic plot of the true stress and true strain by linear regression.

A of bending experiments have been used to reveal bending characteristics of sheet metals. Most of such tests use two-dimensional geometry for simplified analysis and the simulation, while also being a representative of many industrial parts. In the case of our experimental investigation three rolls bending test was used (Fig. 3). The set-up mounted on the testing machine, instrumentation and process control system allows the rig to operate in displacement as well as load control. As in tensile testing three types of specimens 25 mm wide were deformed:

- continuously to determine bending force characteristic,
- progressively to determine springback characteristic – loaded and unloaded by suitable punch motion – up to nearly 70 mm deflection.

The specimen shape at corresponding bending stage was recorded using the digital photo-camera and stored as .jpg files. Using professional computer code GIMP, the .jpg files were elaborated in order to determine changes in a specimen shape, caused by springback phenomenon, and then the springback coefficient was calculated as:

$$K = \frac{R_a}{R_s} \tag{2}$$

where: R_a – radius in active phase of bending (under pressure),
R_s – radius in passive phase of bending (after springback).

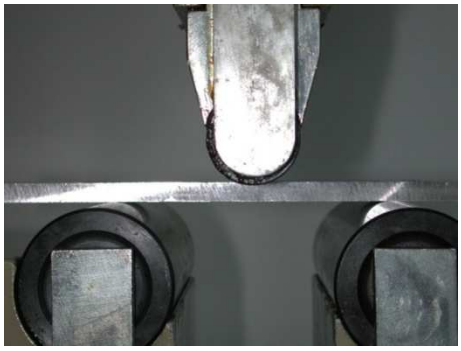

Fig. 3. Scheme of the three rolls bending test

3. Results and discussion

The results of uniaxial tensile of the 18G2A-E355 steel strips (Table 1 and Fig. 4) demonstrate the visible effect of weld presence in the tested specimen. In comparison with base material characteristic, in the case of welded material characteristic it could be noticed that:

- the presence of weld reduces the value of both the uniform and total elongation, especially in the case of the specimen with transverse weld,
- the value of ultimate strength of specimen with longitudinal weld are higher while that of the specimen with transverse weld are smaller,
- the presence of weld resulted in smaller value of the strain hardening exponent.

Table 1. Mechanical properties of the 18G2A-E355 steel specimens

Specimen type	R_e **[MPa]**	R_m **[MPa]**	A_{50} **[%]**	C **[MPa]**	n
Base material	308	510	21	593	0.19
Longitudinal weld	354	544	19	637	0.15
Transverse weld	321	480	16	558	0.14

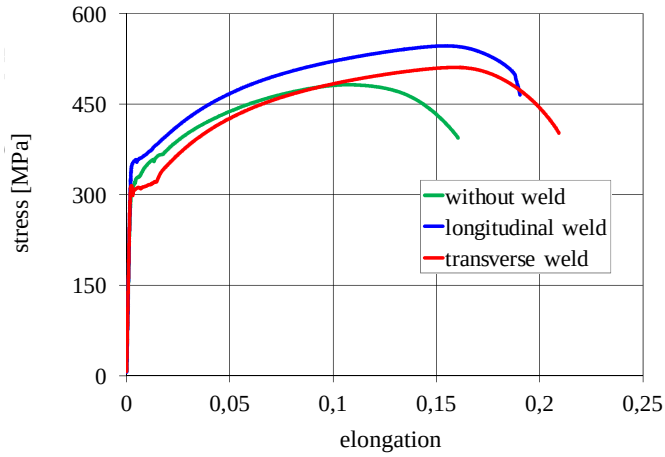

Fig. 4. Flow characteristics of the 18G2A-E355 steel specimens

The highest value of the yield stress and ultimate strength in the case of longitudinal weld resulted from the presence of hard material zone in the centre of weld along the whole specimen in loading direction. The lowest value of the ultimate strength as well as ultimate strain resulted from the presence of two weak material zones located near the weld and oriented transverse to specimen loading. It was confirmed by the strain localisation and specimen failure closed to the weld region.

The bending characteristics, i.e. the relation between bending force and curvature, demonstrate similar run, both in the case of the base material specimen and specimen with longitudinal or transverse weld (Fig. 5). At the first elastic stage of bending, the bending force increases linearly with curvature increase. At the elastic-plastic range of bending the bending force still increases with bending curvature due to strain hardening of a material, and reaches its maximum. At the next stage the bending force started to decrease, as a result of cross-section reduction. The presence of the weld resulted in bending force increasing in the whole range of curvature. This effect is more visible in the case of specimen with longitudinal weld. For the strip with transverse weld the intensity of bending force decrease at the last stage of bending was the most visible.

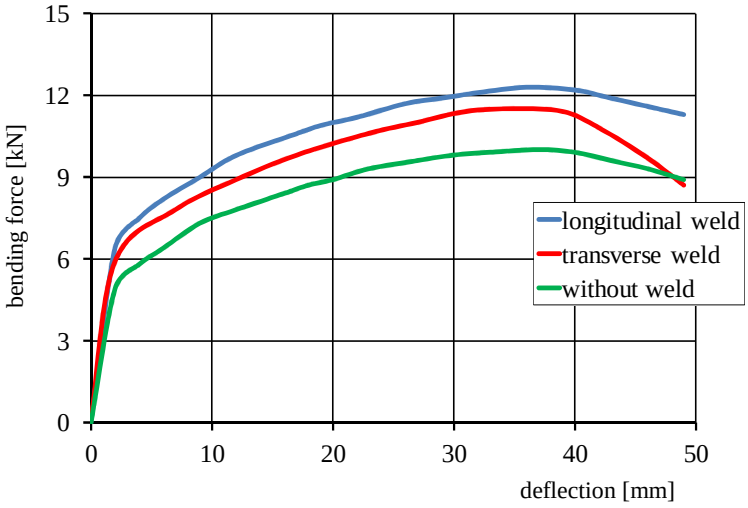

Fig. 5. Bending force characteristics of the 18G2A-E355 steel specimens

The results of springback coefficient calculation were plotted as a function of bending radius (under loading), it means as springback characteristic (Fig. 6). From this presentation it is visible that the value of springback coefficient increases with bending process proceeding, what is a result of elastic zone decreasing in the centre of sheet thickness. The visible change in the springback charecteristic position in comparison with the base material specimen was observed in the case of specimen with longitudinal weld. The presence of transverse weld resulted in slightly larger springback phenomennon, it means smaller value of springback coefficient.

The visible change in springback characteristic in the case of the specimens with longitudinal weld in comparison with that of based material resulted mainly

from the presence of hard material zone in the centre of weld located along whole specimen length and oriented along the bending curvature. In the case of the transverse weld, lower values of the springback coefficient in comparison with that of the based material are observed. It seemed to be the result of transverse orientation of the weld (with one hard and two weak material zones) according to the bending curvature and the location of the weld in the region of the bending punch nose.

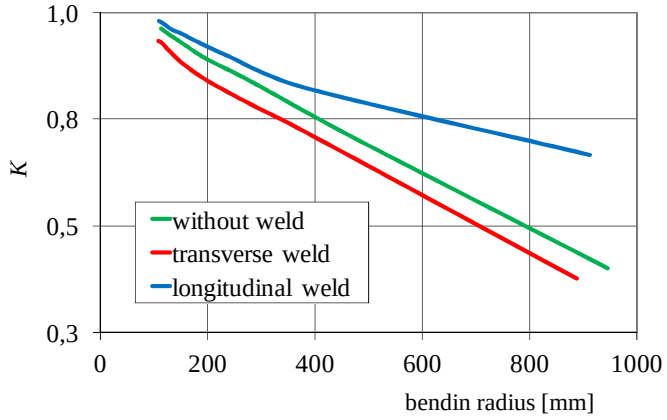

Fig. 6. Springback characteristic of the 18G2A-E355 steel specimens

4. Conclusion

As it should be expected the presence of welding zone in the tested material has the visible effect on both the tensile flow and bending characteristics. The presence of the weld resulted in the bending force increase in the whole range of curvature especially in the case of the specimen with longitudinal weld. Taking into account the springback phenomenon in the case of longitudinal weld this effect could be treated as positive, mainly due to higher value of the springback coefficient in the whole range of bending radius. The presence of transverse weld resulted in decrease of flow characteristic as well as the springback phenomenon is more visible in comparison with the base material (the specimen without any weld).

References

[1] Marciniak Z.: Mechanika procesów tłoczenia blach, WNT, Warszawa 1961.
[2] Lange K.: Handbook of metal forming, McGraw-Hill Company, New York 1985.

[3] Świątkowski K., Stachowicz F.: Analysis of the cross-sectional deformation of box profiles subjected to bending, J. Mech. Work. Technol., 10 (1984), 103-116.
[4] Stachowicz F.: Bending with upsetting of copper tube elbows, J. Mech. Work. Technol., 100 (2000), 236-240.
[5] Stachowicz F., Litwin P., Frącz W.: Experimental and numerical study of open structural profile bending process, Arch. Metall. Mat., 50 (2005), 893-907.
[6] Huang Y-M., Leu D-W.: Effects of process variables on V-die bending process of steel sheet, Int. J. Mech. Sci., 40 (1998), 631-644.
[7] Krywult B., Kawalec S., Stachowicz F.: Automatyczna korekcja krzywizny materiału przy gięciu sprężysto-plastycznym, Mechanik, 53 (1980), 286-287.
[8] Lee S.W., Yang D.Y.: An assessment of numerical parameters influencing springback in explicit finite element analysis of sheet metal forming process, J. Mech. Work. Technol., 80-81, 1998, 60-67.
[9] Stachowicz F.: Experimental and numerical study springback problems in sheet metal bending, Arch. Metall., 48 (2003), 161-172.
[10] Frącz W., Stachowicz F.: Springback phenomenon in sheet metal V-die air bending – experimental and numerical study, Manuf. Eng., 7 (2008), 34-37.
[11] Chalal H., Racz S-G., Balan T.: Springback of thick sheet AHSS subjected to bending under tension, Int. J. Mech. Sci., 59 (2012), 104-114.
[12] Lim H., Lee M.G., Sung J.H., Kim J.H., Wagoner R.H.: Time-dependent springback of advanced strength steels, Int. J. Plasticity, 29 (2012), 42-59.
[13] Abdullah K., Wild P.M., Jeswiet J.J., Ghasempoor A.: Tensile testing for weld deformation properties in similar gage tailor welded blanks using the rule of mixtures, J. Mech. Work. Technol., 112 (2001), 91-97.
[14] Sunar M., Yilbas B.S., Boran K.: Thermal and stress analysis of a sheet metal in welding, J. Mech. Work. Technol., 172 (2006), 123-129.
[15] Chang S.H., Shin J.M., Heo Y.M., Seo D.G.: J. Mech. Work. Technol., 130-131 (2002), 14-19.
[16] Daxin E., Liu Y.: Springback and time-dependent springback of 1Cr18Ni9Ti stainless steel tubes under bending, Materials Design, 31 (2010), 1256-1261.

Experiments were performed using aperture completed thanks to financial support of UDA-RPPK.01.03.00-18-003/10 and POPW 01.03.00-18-012/09-00 and co-financed by the European Union from the European Regional Development Fund within Regional Operational Programme for the Podkarpackie Region for the years 2007-2013.

SIŁA GIĘCIA ORAZ SPRĘŻYNOWANIE W PROCESIE GIĘCIA SPAWANYCH PASM ZE STALI 18G2A-E355

Streszczenie

W wielu opracowaniach można znaleźć znaczną liczbę informacji dotyczących możliwości gięcia, rodzaju uszkodzeń oraz sprężynowania w procesie gięcia blach jednorodnych oraz łączonych przez spawanie. Jednakże dokładne określenie wielkości powrotnych odkształceń sprężys-

tych nadal wymaga dalszych badań, szczególnie w przypadku gięcia blach grubych. Celem prezentowanych badań eksperymentalnych było określenie siły oraz współczynnika sprężynowania podczas gięcia spawanych pasm ze stali 18G2A-E355. W szczególności skoncentrowano się na porównaniu różnic właściwości mechanicznych oraz charakterystyk gięcia blach jednorodnych oraz spawanych uzyskanych w takich samych warunkach testów. Przyrząd do gięcia zamontowany na maszynie wytrzymałościowej, czujniki oraz system pomiarowy umożliwiały rejestrację przemieszczenia oraz siły gięcia. Spawanie pasm blach przeprowadzono metodą MAG w atmosferze CO_2.

Słowa kluczowe: blachy łączone – spawane, umocnienie odkształceniowe, siła gięcia, sprężynowanie

DOI: 10.7862/rm.2012.7

ZESZYTY NAUKOWE POLITECHNIKI RZESZOWSKIEJ **Nr 284**
Mechanika z. 84 (4/12) **2012**

Marek KROK
Janusz PORZYCKI
Roman WDOWIK
Politechnika Rzeszowska

PARAMETRYCZNE PROGRAMOWANIE SZLIFOWANIA WYROBÓW CERAMICZNYCH O ZŁOŻONEJ GEOMETRII

Wytwarzanie wyrobów z ceramiki technicznej o złożonej geometrii wymaga zastosowania maszyn CNC o określonych możliwościach technologicznych, specjalnych narzędzi ściernych oraz właściwie opracowanych programów sterujących. W artykule pokazano parametryczne programowanie obróbki przedmiotów wykonanych z ceramiki technicznej na szlifierce do wałków z osią C sterowaną numerycznie. Przedstawiono również analizę czasu obróbki typoszeregu części o sparametryzowanej geometrii.

Słowa kluczowe: programowanie parametryczne, szlifowanie, szlifierka CNC, wyroby ceramiczne

1. Wprowadzenie

Zapotrzebowanie na wyroby ceramiczne o złożonej geometrii prowadzi do potrzeby doskonalenia maszyn technologicznych sterowanych numerycznie oraz realizowanych na nich procesów obróbki. Ponieważ obróbka ceramiki technicznej po końcowym spieczeniu (rys. 1.) jest możliwa przez zastosowanie procesów obróbki ściernej, doskonalenie tych procesów staje się istotnym zagadnieniem współczesnej technologii obróbki ceramiki [1-3].

Ze względu na duży popyt ze strony krajowych i zagranicznych przedsiębiorstw na ceramiczne części maszyn o złożonych kształtach (rys. 2.), przy braku wytycznych prowadzenia obróbki, oraz potrzebę podnoszenia efektywności (w tym wydajności) procesów, przed przedsiębiorstwami związanymi z produkcją ceramicznych części maszyn są stawiane wyzwania technologiczne polegające na opracowaniu i wdrażaniu właściwych technologii, które umożliwią reagowanie na potrzeby rynku oraz spowodują ich dalszy rozwój.

Rys. 1. Przebieg procesu technologicznego dla wyrobów ceramicznych
Fig. 1. The course of technological process of ceramic products

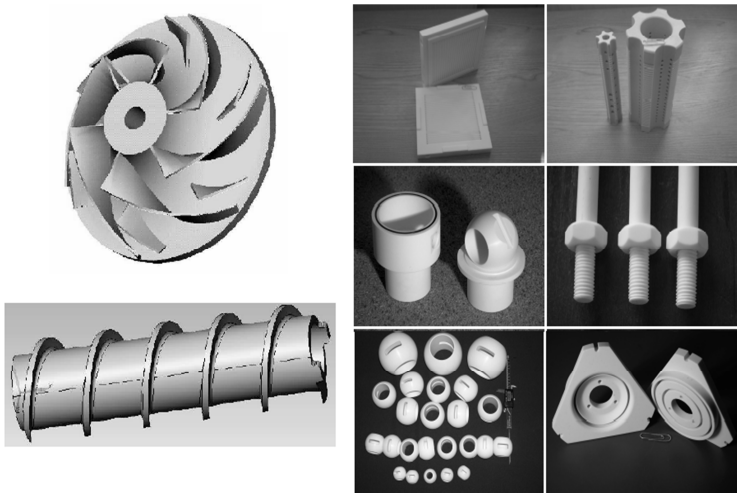

Rys. 2. Przykłady ceramicznych wyrobów o złożonej geometrii, opracowano na podstawie [4]
Fig. 2. Examples of ceramic products with complex geometry, prepared on the basis of [4]

2. Wytwarzanie wyrobów z ceramiki na szlifierce CNC do wałków

Przykładem wyrobów ceramicznych, których produkcja seryjna lub wielkoseryjna może w niedalekiej przyszłości osiągać znaczące wyniki, są przedmioty z owalnym zarysem przekroju. Są one wykonywane na szlifierkach do wałków

(rys. 3.), których kinematyka umożliwia sterowanie ruchem punktu charakterystycznego ściernicy względem układu współrzędnych przedmiotu w osiach prostoliniowych X i Z oraz osi obrotowej C (rys. 5.). Ważnym zagadnieniem w produkcji wyrobów ceramicznych jest konieczność efektywnej obróbki części podobnych, tzn. typoszeregu wyrobów o różnych wymiarach. Rysunek 3. przedstawia przykładowy przedmiot obrabiany z ceramiki technicznej, który może stanowić wybrany element z typoszeregu wymiarowego pokazanego na rys. 6.

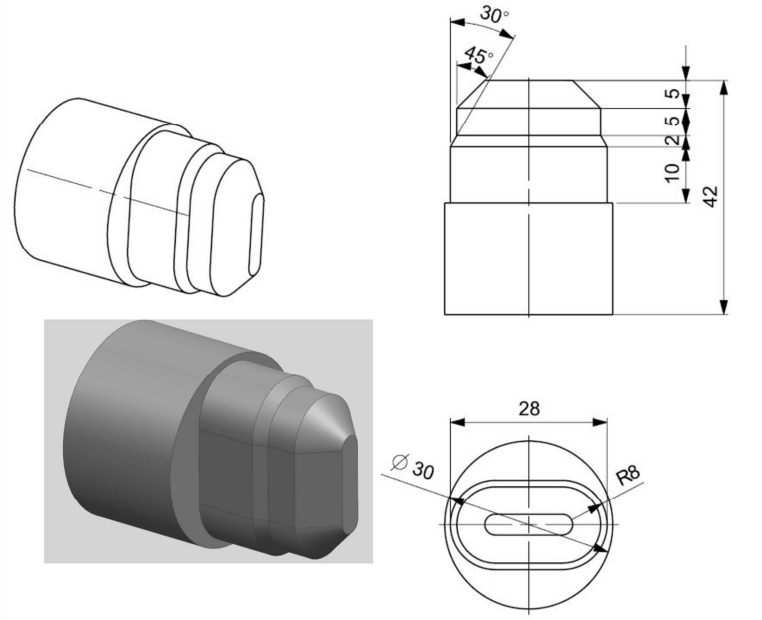

Rys. 3. Przykładowy przedmiot obrabiany z ceramiki technicznej
Fig. 3. Example of a workpiece made of technical ceramic

3. Szlifierka CNC RUP 28 z układem Sinumerik 840Di

W Katedrze Technik Wytwarzania i Automatyzacji Politechniki Rzeszowskiej została wdrożona (w 1992 r.) szlifierka typu RUP 28 z prototypowym polskim układem CNC NUMS 740. Wdrożenie szlifierki było wynikiem realizacji wielu prac w ramach CPBR 6.1 cel 70.4. Aby możliwe było wykorzystanie szlifierki RUP 28 do prac badawczych i produkcyjnych, konieczna była jej modernizacja (ze względu na przestarzały układ sterujący) i zastosowanie nowoczesnego układu CNC. Do sterowania obrabiarki wykorzystano układ CNC Sinumerik 840Di (rys. 4.), który umożliwia sterowanie osiami prostoliniowymi X i Z oraz osią obrotową C (rys. 5.).

Rys. 4. Szlifierka RUP 28 z układem CNC Sinumerik 840Di
Fig. 4. RUP 28 grinding machine with CNC Sinumerik 840Di control

a)

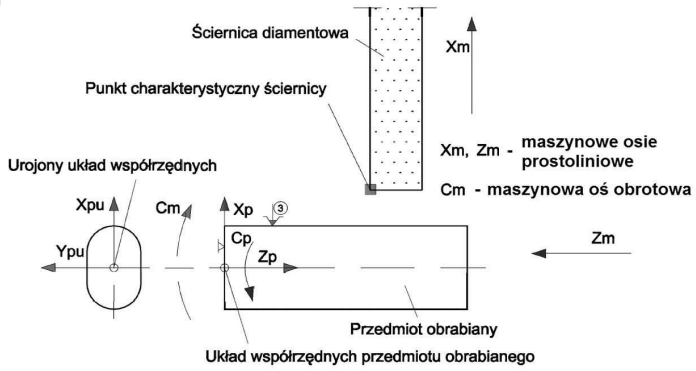

b)

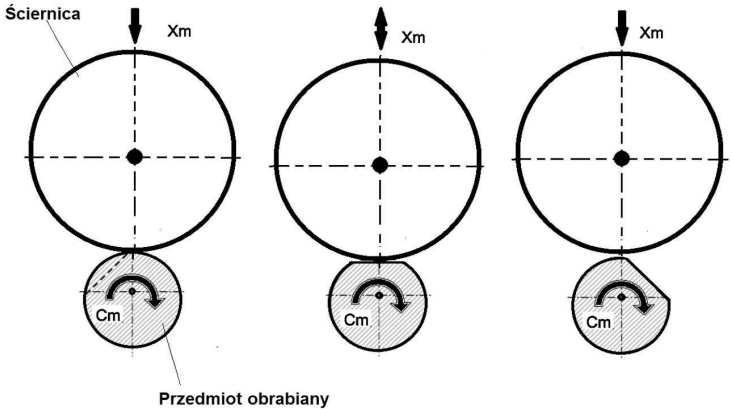

Rys. 5. Obróbka z osią maszynową Cm na szlifierce RUP 28 CNC: a) osie maszynowe i układy współrzędnych, b) zasada obróbki konturu podczas sprzężenia osi maszynowych Xm i Cm
Fig. 5. Machining with Cm machine axis on RUP 28 CNC grinding machine: a) axes and coordinate systems, b) principle of contour machining (coupling of Xm and Cm axes)

4. Programowanie obróbki typoszeregu wyrobów o sparametryzowanej geometrii

4.1. Typoszereg wymiarowy wyrobów ceramicznych

Przykładowy typoszereg wymiarowy wyrobów ceramicznych (odniesiony do przedmiotu z rys. 3.) przedstawia rys. 6. Dwanaście wyrobów (od M1 do M12) różni się promieniem zaokrąglenia części środkowej (od R13 do R2), co diametralnie zmienia kształt wyrobów i wpływa znacząco na przebieg procesu obróbki.

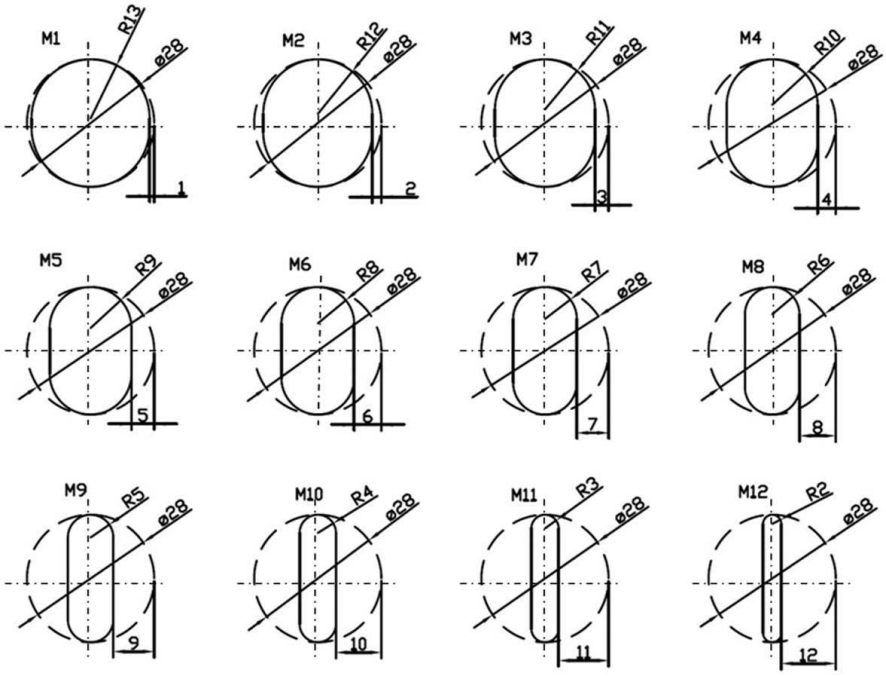

Rys. 6. Typoszereg wymiarowy wyrobów ceramicznych
Fig. 6. Type dimension of ceramic products

4.2. Sparametryzowany program sterujący

Programowanie toru ruchu ściernicy dla szlifierki RUP 28 CNC może odbywać się przez zastosowanie osi prostoliniowych w układzie prostokątnym lub biegunowym, natomiast programowanie ruchu z dodatkową osią C przez zadawanie współrzędnych końca ruchu osi C, X, Z lub przez zastosowanie funkcji TRANSMIT, co opisano w pozycjach [5, 6]. Na rysunku 7. wyjaśniono parametry przyjęte do opracowania programu obróbki typoszeregu części z rys. 5.

W tabeli 1. przedstawiono opracowany program sterujący (główny i podprogram) przeznaczony do obróbki typoszeregu wyrobów określonych sparametryzowaną geometrią z rys. 7. dla szlifierki RUP 28 CNC z układem Sinumerik 840Di.

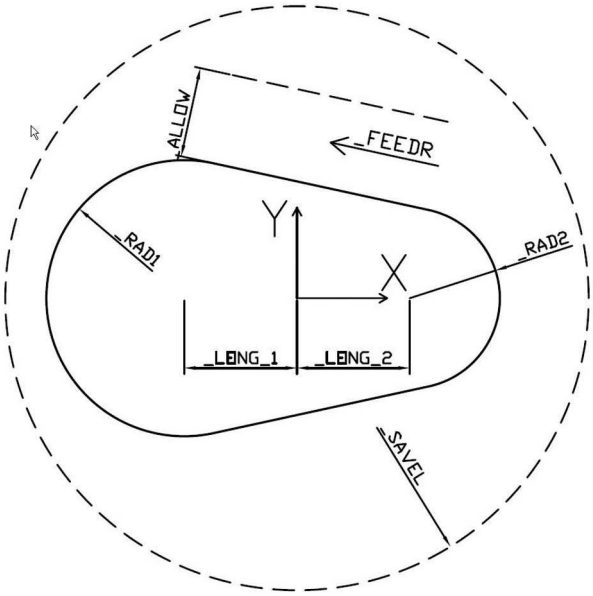

Rys. 7. Rysunek pomocniczy do opracowania programu obróbki
Fig. 7. Auxilary draft to work out of machining program

Tabela 1. Program główny %_N_PROG_MPF oraz podprogram %_N_PROG_SPF
Table 1. Main program %_N_PROG_MPF and subprogram %_N_PROG_SPF

%_N_PROG_MPF EXTERN CYCLE_CAM(REAL,REAL,REAL,REAL,REAL,REAL,REAL,REAL,REAL,REAL) G54 WORKPIECE(,,,"CYLINDER",0,0,-20,-10,30) T="CUTTER" ;T="PLUNGE_CUTTER_3 A" ;T="ROUGHING_T80 A" SETMS(3) S4000 M3 CYCLE_CAM(-1,13,1,13,1,0,0.01,2,4000,10) SPOS[1]=90 **M30**
%_N_PROG_SPF N10 PROC CYCLE_CAM(REAL _LEVEL, REAL _RAD1, REAL _LENG1, REAL _RAD2, REAL _LENG2, REAL _ANG, REAL _AP, REAL _ALLOW, REAL _FEEDR, REAL _SAVEL) SAVE ; DEFINICJA CYKLU WRAZ Z TYPEM ORAZ NAZWĄ PRZYJMOWANYCH PARAMETRÓW: ; _LEVEL - POZYCJA W OSI WZDŁUŻNEJ ; _RAD1, _RAD2 - PROMIENIE ZAOKRĄGLENIA KRZYWKI ; _LENG1, _LENG2 - POŁOŻENIA ŚRODKÓW OKRĘGÓW KRZYWKI

```
; _ANG - KĄT SKRĘCENIA KRZYWKI WZGLĘDEM OSI X
; _AP - DOSUW NA OBRÓT
; _ALLOW - NADDATEK DO USUNIĘCIA
; _FEEDR - POSUW/ PRĘDKOŚĆ OBWODOWA PRZEDMIOTU OBRABIANEGO
; _SAVEL - ODLEGŁOŚĆ BEZPIECZNA
N20 DEF AXIS _PLANE=Z
N30 DEF AXIS _LIN=X
N40 DEF AXIS _CIR=SP1
; DEFINICJA OSI W PRZYPADKU ZASTOSOWANIA CYKLU NA INNEJ OBRABIARCE
N50 DEF INT _NOP, _I
; DEFINICJA ZMIENNYCH POMOCNICZNYCH
; _NOP - LICZBA PRZEJŚĆ
; _I - LICZNIK WYKONANYCH PRZEJŚĆ
N60 _I=0
; KASOWANIE LICZNIKA _I
N70 G17
; WYBÓR PŁASZCZYZNY KOREKCJI
N80 DIAMOF
; WYŁĄCZENIE WYMIAROWANIA W ŚREDNICACH
N90 G0 AX[_PLANE]=_LEVEL
N100 G0 AX[_CIR]=90
; NAJAZD NA POZYCJĘ PRACY
N110 F=_FEEDR
; USTAWIENIE POSUWU
N120 _NOP=ROUND(_ALLOW/_AP)
; OBLICZENIE ILOŚCI PRZEJŚĆ
N130 TRANSMIT
; WŁĄCZENIE TRANSFORMACJI OSI X, Y NA OSIE X, C
N140 OFFN=(_AP*(_NOP-_I))
; USTAWIENIE ODSUNIĘCIA OD KONTURU
N150 G1 X=-(_SAVEL+_ALLOW+_LENG1) Y=_RAD2 G41
; NAJAZD NA PROFIL
N160 PROFILE:
N170 MSG("POZOSTALO NR: " << (_NOP-_I))
; WYŚWIETLENIE KOMUNIKATU INFORMACYJNEGO O POZOSTAŁEJ ILOŚCI PRZEJŚĆ
N180 G1 X=_LENG2 Y=_RAD2
N190 G2 X=_LENG2 Y=-_RAD2 I=AC(_LENG2) J=AC(0)
N200 G1 X=-_LENG1 Y=-_RAD1
N210 G2 X=-_LENG1 Y=_RAD1 I=AC(-_LENG1) J=AC(0)
; OBRÓBKA KONTURU
N220 _I=_I+1
; ZWIĘKSZENIE LICZNIKA
N230 OFFN=(_AP*(_NOP-_I))
; DOSUNIĘCIE DO KONTURU O _AP
N240 REPEAT PROFILE P=_NOP
; POWTÓRZENIE PROFILU OKREŚLONĄ ILOŚĆ RAZY
N250 G1 X=_SAVEL+_ALLOW+_LENG1 Y=_RAD2 G40
; ODJAZD OD KONTURU
N260 TRAFOOF
; WYŁĄCZENIE TRANSFORMACJI
N270 M17
```

Aby sprawdzić program obróbki, należy dokonać jego symulacji. Na rysunku 8. przedstawiono ekran układu Sinumerik 840Di, na którym jest widoczny tor ruchu punktu charakterystycznego ściernicy podczas symulacji obróbki jednego

z przedmiotów ich typoszeregu. Na podstawie symulacji można określić czas obróbki przedmiotu.

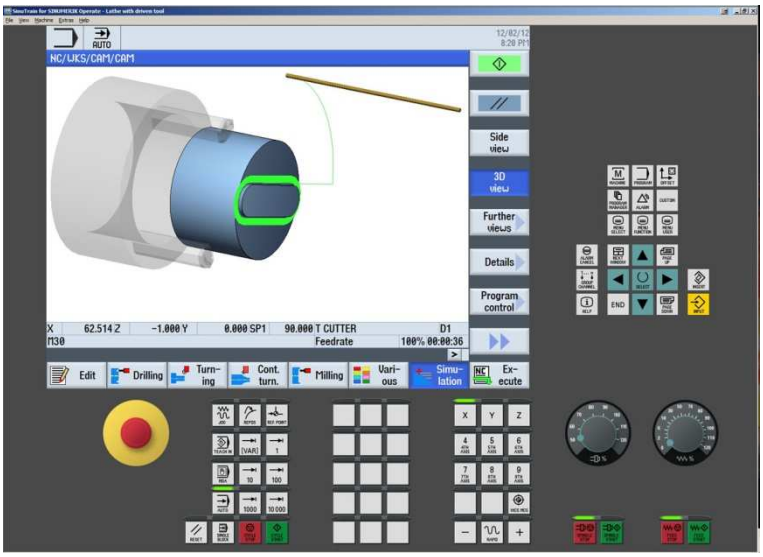

Rys. 8. Ekran symulatora układu Sinumerik 840Di
Fig. 8. Screen of Sinumerik 840Di simulator

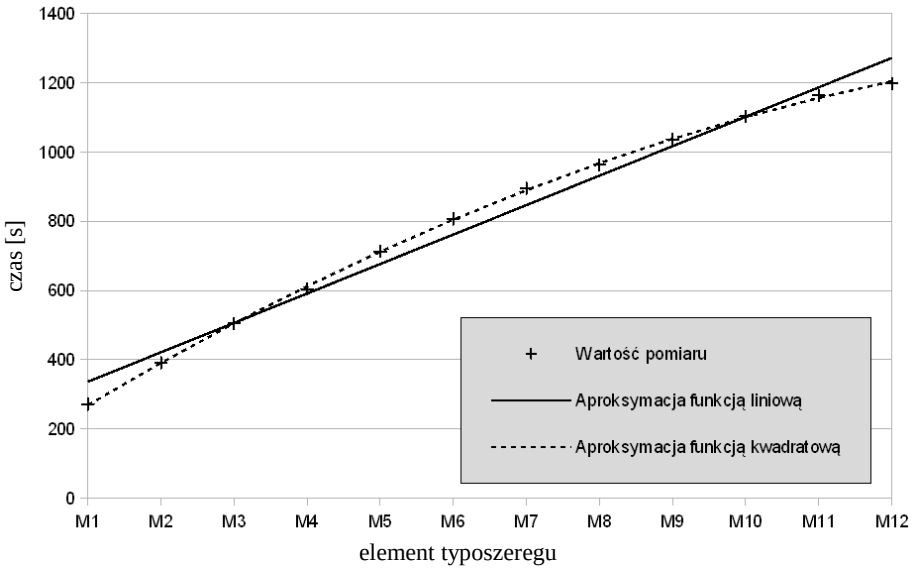

Rys. 9. Czas obróbki typoszeregu wyrobów
Fig. 9. Time of machining of type dimension products

4.3. Analiza czasu obróbki

Ważnym czynnikiem podczas planowania produkcji danego wyrobu jest znajomość głównego czasu obróbki. Rysunek 9. przedstawia czas obróbki typoszeregu części (od M1 do M12) z rys. 6. dla tych samych parametrów technologicznych. Zmienny czas wynika z różnicy drogi, jaką przebędzie punkt charakterystyczny ściernicy względem przedmiotu obrabianego podczas obróbki poszczególnych przedmiotów za pomocą tego samego sparametryzowanego programu obróbkowego.

5. Podsumowanie

Ceramika techniczna ze względu na swoje właściwości użytkowe coraz częściej znajduje zastosowanie jako materiał konstrukcyjny. Obróbka wyrobów z ceramiki nie jest jednak łatwa, gdyż materiał ten należy do trudno obrabialnych. Z tego powodu szczególnie obróbka wykończeniowa jest realizowana za pomocą szlifowania z użyciem ściernic diamentowych. Wyroby ceramiczne o złożonej geometrii wymuszają także stosowanie do ich obróbki zaawansowanych wieloosiowych maszyn CNC, dla których konieczne jest właściwe opracowanie programu sterującego. Zastosowanie programowania parametrycznego upraszcza program sterujący, skraca jego długość, a przede wszystkim umożliwia obróbkę typoszeregu wyrobów za pomocą tego samego programu z różnymi wartościami parametrów. Ten sposób programowania upraszcza również wyznaczanie czasu obróbki każdego przedmiotu ze zbioru objętego typoszeregiem wyrobów, co ma znaczenie podczas planowania produkcji. Mimo doskonalenia różnych sposobów obróbki skrawaniem materiałów w stanie twardym, można twierdzić, że szlifowanie nadal zachowuje zdolność konkurowania z nimi dzięki stałemu postępowi zachodzącemu w budowie ściernic, szlifierek i w stosowanych procesach [7]. W odniesieniu do ceramiki technicznej po końcowym spieczeniu jest ona przykładem efektywnej techniki jej obróbki ubytkowej.

Literatura

[1] Manison P.: Technical ceramics – tough benefits, World Pumps, May 2009.
[2] Liang Y., Dutta S.P.: Application trend in advanced ceramic technologies, Technovation, 21 (2001), 61-65.
[3] Oczoś K.E.: Kształtowanie ceramicznych materiałów technicznych, Oficyna Wydawnicza Politechniki Rzeszowskiej, Rzeszów 1996.
[4] Materiały informacyjne firmy CEREL, http://www.cerel.eu.
[5] Stryczek R., Pytlak B.: Elastyczne programowanie obrabiarek, Wydawnictwo Naukowe PWN, Warszawa 2011.
[6] http://support.automation.siemens.com.
[7] Porzycki J.: Modelowanie szlifowania osiowego zewnętrznych powierzchni walcowych, Oficyna Wydawnicza Politechniki Rzeszowskiej, Rzeszów 2004.

PARAMETRIC PROGRAMMING OF GRINDING OF CERAMIC PRODUCTS WITH COMPLEX GEOMETRY

A b s t r a c t

Machining of technical ceramic products requires application of CNC machines which have predetermined technological possibilities, special grinding tools and properly made control programs. In this paper parametric programming of ceramic products machining using CNC grinding machine with C axis is described. Time analysis of machining of type dimension ceramic products with parametric geometry is also presented.

Keywords: parametric programming, grinding, CNC grinding machine, ceramic products

DOI: 10.7862/rm.2012.8

ZESZYTY NAUKOWE POLITECHNIKI RZESZOWSKIEJ **Nr 284**
Mechanika z. 84 (4/12) **2012**

Andrzej SKRZAT
Rzeszow University of Technology

APPLICATION OF COUPLED EULERIAN-LAGRANGIAN APPROACH IN METAL FORMING SIMULATIONS

Numerical simulations of materials forming processes require both powerful computers and advanced software. Large displacements assumed in the analysis usually cause convergence problems. In the Lagrangian approach (typical for solid bodies) a remeshing is frequently necessary. This extends the computations and decreases the convergence. In such cases the application of Euler approach (typical for fluid flows) is an practical alternative. In the Euler approach the finite elements mesh remains fixed, while material flows through it. There is no need for remeshing, therefore. In this paper selected results of coupled Eulerian-Lagrangian analysis are presented. A bent beam as the benchmark test and backward extrusion as an example of metal forming process are considered. Some models parts (tools) are described by updated Lagrangian formulation, other parts (material) are described by Eulerian approach. Obtained results of CEL analyses were compared to ones of the pure Lagrangian approach.

Keywords: coupled Eulerian-Lagrangian, large displacements, metal forming

1. Introduction

Lagrangian and Eulerian approaches are commonly used in simulations of large displacement problems of solid mechanics. Both formulations have their advantages and limitations. In the Total Lagrangian approach (TL) the initial configuration for the time $t = 0$ and the final state for the time $t + \Delta t$ are considered. In the Updated Lagrangian approach (UL) the configurations for the time $t + \Delta t$ are referred to the solution obtained for the time t (Fig. 1).

Unfortunately, as the finite element mesh becomes distorted under the loading, the generation of completely new mesh is required more or less frequently. It causes convergence problems and extends the computation time. In such cases the Eulerian approach becomes more efficient than Lagrangian approach. In the Eulerian formulation the finite element mesh remains fixed, while material flows through it. There is no need for remeshing, therefore. In the ninetieths Lagrangian and Eulerian approaches were combined together in the new approach called coupled Eulerian-Lagrangian (CEL). The CEL method was initially applied to

fluid-structure interaction problems. In Figure 2 the results of the water-filled bottle drop-test are presented. The bottle strikes the floor at a skew angle, with one of the bottom corners experiencing the initial impact. A simulation for the bottle accounts both the exterior forces on the bottle from the floor impact, as well as the interior forces of the water pushing against the bottle. Coupled Eulerian-Lagrangian approach may be also applied to metal forming problems. In Figure 3 presented are the results of Lagrangian and CEL rivet forming simulations. Rivets are designed to create permanent attachments between two or more

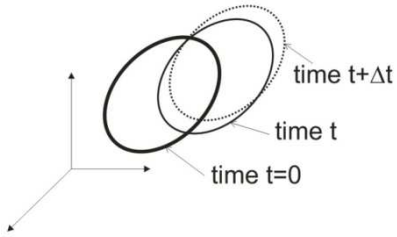

Fig. 1. Reference frames for total Lagrangian and updated Lagrangian

Fig. 2. The water-filled bottle drop-test (CEL model)

a) b)

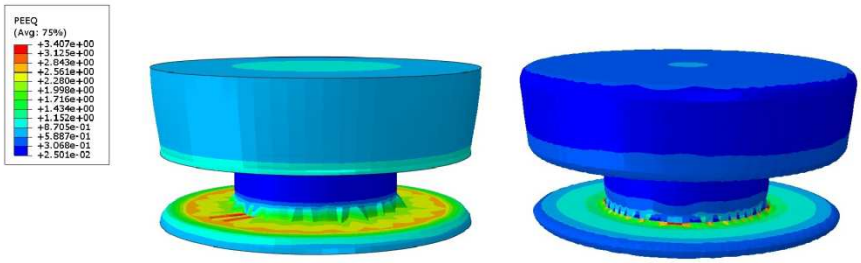

Fig. 3. Equivalent plastic strains in the rivet forming simulation – Lagrangian (a) and CEL (b) analyses

sheets of material. After both ends of the rivet are compressed the diameter of the rivet body expands, pinching the sheets of material between the two ends of the rivet. The rivet is modeled by Eulerian elements while tools are Lagrangian elements. In both exemplary simulations Lagrangian and Eulerian elements are combined simultaneously in the same model. In the CEL analyses bodies that undergo large deformations are meshed with Eulerian elements, while stiffer bodies in the model are meshed with more efficient Lagrangian elements.

2. Overview of coupled Lagrangian-Eulerian formulation

In the Eulerian description equations are written using spatial time derivatives. In the standard Lagrangian description material time derivatives are used. The relation between material and spatial time derivatives is:

$$\frac{D\Phi}{Dt} = \frac{\partial \Phi}{\partial t} + \mathbf{v} \cdot (\nabla \Phi) \tag{1}$$

where: Φ – the arbitrary solution variable, $\mathbf{v}$ – the material velocity. $\frac{D\Phi}{Dt}$ and $\frac{\partial \Phi}{\partial t}$ are the material and spatial time derivatives, respectively.

The Lagrangian mass, momentum and energy conservation equations transferred into the Eulerian (spatial derivatives) conservation equations [1] are:

$$\frac{\partial \rho}{\partial t} + \mathbf{v} \cdot (\nabla \rho) + \rho \nabla \cdot \mathbf{v} = 0 \tag{2}$$

$$\frac{\partial \mathrm{v}}{\partial t} + \mathbf{v} \cdot (\nabla \cdot \mathbf{v}) = \frac{1}{\rho}(\nabla \cdot \boldsymbol{\sigma}) + \mathbf{b} \tag{3}$$

$$\frac{\partial e}{\partial t} + \mathbf{v} \cdot (\nabla e) = \boldsymbol{\sigma} : \mathbf{D} \tag{4}$$

where: ρ – the density, $\boldsymbol{\sigma}$ – the Cauchy stress, $\mathbf{b}$ – the vector of body forces, e – the strain energy, $\mathbf{D}$ – the velocity strain.

The Eulerian equations (2)-(4) can be written in the conservative forms:

$$\frac{\partial \rho}{\partial t} + \nabla \cdot (\rho \mathrm{v}) = 0 \tag{5}$$

$$\frac{\partial \rho \mathbf{v}}{\partial t} + \nabla \cdot \left(\rho \mathbf{v} \otimes \mathbf{v} \right) = \nabla \cdot \boldsymbol{\sigma} + \rho \mathbf{b} \tag{6}$$

$$\frac{\partial e}{\partial t} + \nabla \cdot \left(e\mathrm{v} \right) = \boldsymbol{\sigma} : \mathbf{D} \tag{7}$$

The Eulerian governing equations (5)-(7) have the general form:

$$\frac{\partial \varphi}{\partial t} + \nabla \cdot \Phi = \mathrm{S} \tag{8}$$

where: Φ – the flux function, S – the source term.

Operator splitting divides Eq. (8) into two equations solved sequentially [2]:

$$\frac{\partial \varphi}{\partial t} = \mathrm{S} \tag{9}$$

$$\frac{\partial \varphi}{\partial t} + \nabla \cdot \Phi = 0 \tag{10}$$

Eq. (9) contains the source term represents the Lagrangian step. Eq. (10) contains the convective term represents the Eulerian step. Graphical representation of the split operator is shown in Fig. 4.

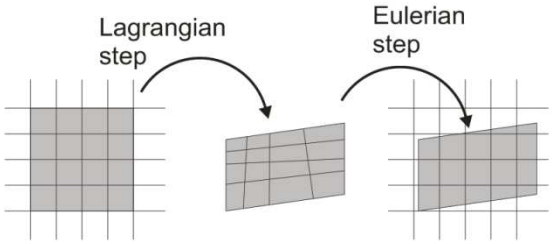

Fig. 4. Split operator for the CEL formulation

To solve Eq. (10) the deformed mesh from Lagrangian step is moved to the Eulerian fixed mesh, and volume of material transported between adjacent elements is calculated. The Lagrangian solution variables (e.g. mass, stress, energy) are adjusted to account for the flow of the material between adjacent elements. For the Lagrangian step the principle of virtual work is applied [3]:

$$\int_V \rho \mathbf{a} \cdot \delta \mathbf{u} \, \mathrm{d}v + \int_V \boldsymbol{\sigma} : \delta \boldsymbol{\varepsilon} \, \mathrm{d}V = \int_S \mathbf{t} \cdot \delta u \, \mathrm{d}S + \int_V \rho \mathbf{b} \cdot \delta \mathbf{u} \, \mathrm{d}V \tag{11}$$

where: $\delta\mathbf{u}$ – the virtual displacement, $\delta\boldsymbol{\varepsilon}$ – the virtual strain resulting from virtual displacements, **a** – the spatial acceleration, and **t** – the surface traction. In the Lagarangian step the updated Lagrangian formulation is suitable because the reference configuration (time t) is the current configuration in the Eulerian approach. Unfortunately, in general the configuration of the body at time $t + \Delta t$ considered in Eq. (11) is unknown (unknown is the volume of integration and density which depends on the body deformations). Moreover, the Cauchy stress at time $t + \Delta t$ cannot be obtained by adding to the Cauchy stress at time t the stress increment because the components of the Cauchy stress tensor change when material is subjected to a rigid body rotation. In practice other strain and stress measures have to be used in the principle of virtual displacements (11) – the Green-Lagrange strain tensor and the second Piola-Kirchoff stress tensor [4]. In order to calculate the material(s) occupation in the Eulerian mesh the volume fraction parameter (VF) is introduced [5]. The initial VF estimation requires the reference volume associated with the fixed regular Eulerian mesh (Fig. 5).

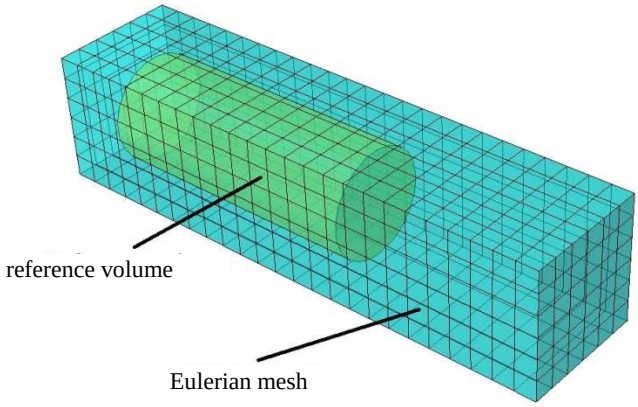

Fig. 5. Reference volume for the volume fraction parameter estimation

3. Benchmark test – the bent beam

The bent beam presented in Fig. 6 is considered as the benchmark test. The beam is modeled by Eulerian elements. The initial occupation of beam in 3D space is defined by the reference volume. The Eulerian part of the model sur-

rounds entirely the beam volume including its later deformations. In Figure 6 one can see two bottom supports and the upper punch being used to apply the load to the beam. Bilinear elastic-plastic material is assumed for the beam. Typically such problems are solved by Lagrangian approach.

The results of the CEL analysis are presented in Fig. 7. The beam deflection and the distribution of stress is similar to ones obtained in pure Lagrangian analysis (not presented here). Unfortunately, in presented CEL analysis all the beam edges are rounded. This is caused by course Eulerian mesh. As a rule, a fine grid resolution comparable with the average radius of geometry curvature is required in Eulerian analyses. External loads can never be applied directly to the Eulerian mesh – contact analysis is the only way to apply a mechanical load

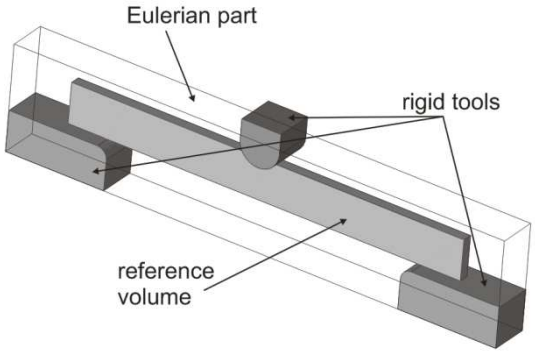

Fig. 6. Bent beam model

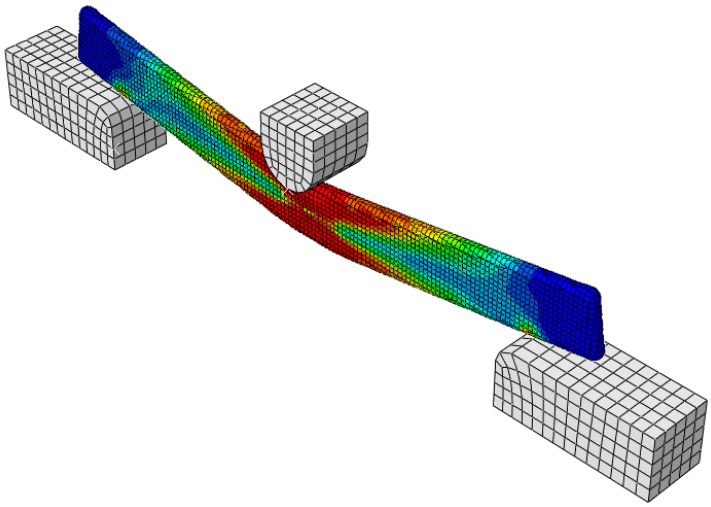

Fig. 7. Equivalent stress in the bent beam CEL analysis

to Eulerian elements. In this test the load is applied to the beam by rigid tools. In the case of other type of loads (e.g. pressure, concentrated force, moment) aditional flexible parts have to be included in the analysis. Auxiliary Lagrangian flexible parts loaded by mechanical forces affect the Eulerian parts by contact interactions.

4. Coupled Eulerian-Lagrangian simulation of backward extrusion

The backward extrusion is a forming process widely used for the manufacturing of solid and hollow parts. The punch strikes the blank extruding it upwards by means of applied high pressure. The analysis of the extrusion forming operations requires evaluation of process parameters such as force and energy consumption as well as the determination of the distribution of the major field variables e.g. plastic strains. Numerical simulations of the backward extrusion process can lead to reduction of forming forces and allow to improve the forming accuracy. Unfortunately, from the mechanical point of view such simulations are very sophisticated. Usually, the finite element mesh becomes very distorted under the load and frequent remeshing is necessary, therefore. Large displacements, contact interactions and remeshing might be the source of convergence problems in Lagrangian analysis. In such cases the Eulerian analysis in which the finite element mesh remains fixed might provide reliable results [6]. The FEM model of the coupled Eulerian-Lagrangian analysis of the backward extrusion process is presented in Fig. 8. The die and recipient are assumed to be rigid bodies. In this simulation the die moves into the cylindrical recipient.

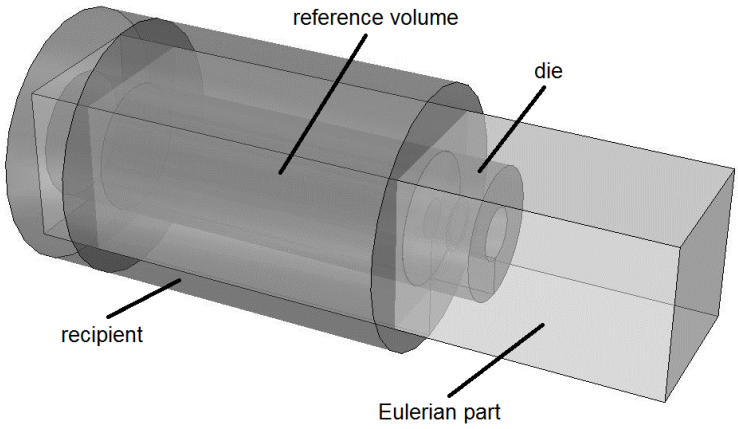

Fig. 8. FEM model of backward extrusion

The processed material is aluminum alloy at 450°C. The stress-plastic strain curve is obtained from [7] for Bodner-Partom material model. Assumed B-P material data are: $D_0 = 10^4$ s^{-1}, $Z_0 = 280$ MPa, $Z_1 = 647$ MPa, $Z_2 = 35$ MPa, $Z_3 = 80$ MPa, $m_1 = 0{,}182$ MPa^{-1}, $m_2 = 3{,}7$ MPa^{-1}, $r_1 = r_2 = 4$, $A_1 = 0{,}15$, $A_2 = 0{,}99$, $n = 1{,}9$. The description of Bodner-Partom material model and its material data is available in [8]. In numerical computations commercial ABAQUS program was used. In ABAQUS program the coupled Eulerian-Lagrangian analysis is restricted to three-dimensional dynamic explicit problems only. Obtained equivalent plastic strain distribution in the extruded bar is shown in Fig. 9. The plot of external work versus the displacement obtained from the simulation is typical for backward extrusion problems (Fig. 10).

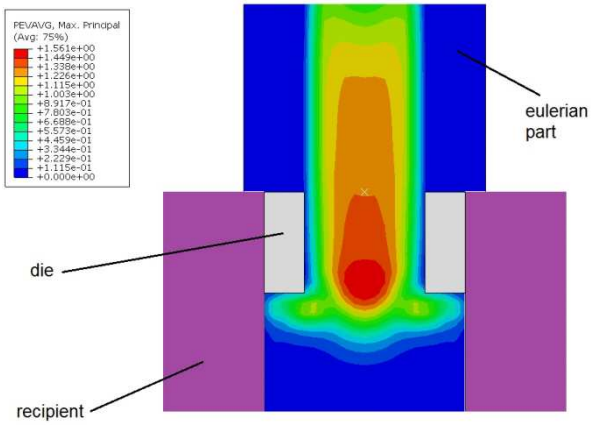

Fig. 9. Equivalent plastic strain distribution in the extruded bar

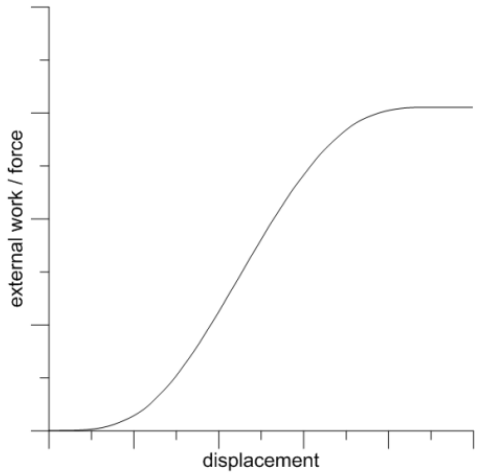

Fig. 10. External work vs. displacement in backward extrusion

Considered problem can be solved more efficiently by axisymmetric Lagrangian analysis. Presented results obtained by the CEL analysis are comparable with the results of appropriate Lagrangian analysis which are not presented here. The effectiveness and stability of the CEL analysis can be demonstrated on extrusion problems in which more complicated extruded shapes are considered. In Fig. 11 the non-symmetric skewed double-tee bar used in the aviation industry is presented. Numerical Lagrangian simulation of the extrusion of this profile provides extreme element distortions, and it is both very time consuming and unstable.

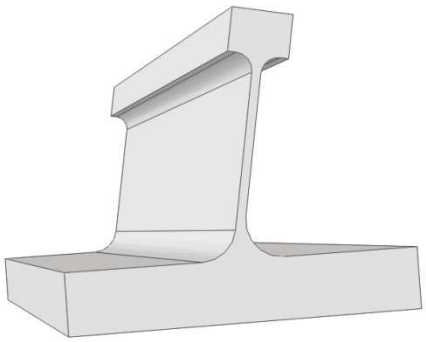

Fig. 11. Special double-tee beam used in aviation industry

Coupled Eulerian-Lagrangian extrusion analysis runs for this profile without any problems. The only limitation is the size of this task. Thin web of an I-beam provides generation of very small Eulerian elements – material cannot flow through several elements in one time/load increment. Moreover, the dynamic explicit procedure applied here is conditionally stable, and requires very small time increments (of order 10^{-6} s) when small finite elements are used. This extends the computation time very much. To solve this problem powerful workstation (12 processors, 24 Gb of memory) run this problem over two weeks. However, computations based on purely Lagrangian approach even if possible for this sophisticated geometry, would take more time. The geometry of extruded element for early stage of the considered backward extrusion problem is presented in Fig. 12. It should be kept in mind that in ABAQUS post processor in the visualization of the CEL analyses all edges are (unfortunately) rounded.

Presented preliminary simulation is useful in the estimation of the size of the problem, required memory and the computation time in numerical simulations of reversed extrusion of sophisticated-shape elements. Results of such simulations will also help in better design of dies.

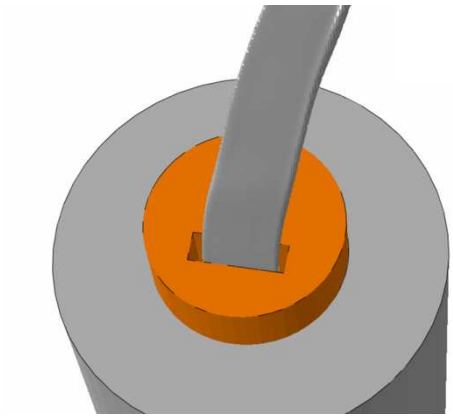

Fig. 12. Backward extrusion of an I-beam profile

5. Conclusion

The coupled Eulerian-Lagrangian approach is a very useful tool for solving large displacement problems. Many tasks which are very hard-to-solve by Lagrangian approach can be successfully solved by the CEL analysis. The CEL solution procedure is very stable even for complicated shapes because the Eulerian finite element mesh remains fixed during analysis. The CEL analysis is restricted only to dynamics problems in which inertia forces are considered. In ABAQUS program only explicit integration of the governing equations is allowed. It limits the application of the CEL analysis to short-term problems. In the dynamic explicit approach the stable time increment is usually very small, thus the long-term analysis would require millions of load increments and in consequence would take weeks or even months on powerful workstations. Presented results are very promising. They are stable independently of the shape of extruded elements. The last presented example is very hard to solve by Lagrangian approach. It was efficiently solved by coupled Eulerian-Lagrangian approach. In the future research the results of computer simulations will be compared with the experimental data. In Department of Material Forming and Processing hundreds of backward extrusion tests have been made for various types of materials, different extruded shapes and various temperature. This valuable experimental information will help to select an appropriate material model – in presented simulation simple bilinear elastic-plastic material model was used. One of the candidates is Bodner-Partom material model which allows to take simultaneously into consideration elastic and plastic effects, isotropic and kinematic hardening, visco-plasticity, creep and relaxation for a wide range of temperature. Application of BP material model in the commercial software (ABAQUS) requires writing user material procedure.

References

[1] Benson D.J., Okazawa S.: Contact in a multi-material Eulerian finite element formulation, Comput. Methods Appl. Mech. Engng., 193 (2004), 4277-4298.
[2] Benson D.J.: A mixture theory for contact in multi-material Eulerian formulations, Comput. Methods Appl. Mech. Engng., 140 (1997), 59-86.
[3] Bathe K.J.: Finite element procedures, Upper Saddle River 1996.
[4] Belytschko T., Liu K.W., Moran B.: Non-linear Finite Element Analysis for continua and structures, New York 2000.
[5] Al-Athel K.S., Gadala M.S.: Eulerian volume of solid (VOS) approach in solid mechanics and metal forming, Comput. Methods Appl. Mech. Engng., 200 (2011), 2145-2159.
[6] Gouveia B.P.P.A., Rodrigues J.M.C., Martins P.A.F.: Finite element modeling of cold forward extrusion using updated Lagrangian and combined Eulerian-Lagrangian formulations, J. Mat. Proc. Technol., 80-81 (1998), 647-652.
[7] Bodner S.R.: Unified plasticity for engineering applications, New York – Boston 2002.
[8] Skrzat A.: Fuzzy logic application to strain-stress analysis in selected elastic-plastic material models, Arch. Metall. Mater., 56 (2011), 559-568.

ZASTOSOWANIE SPRZĘŻONEGO PODEJŚCIA EULERA-LAGRANGE'A W SYMULACJACH PROCESÓW PRZERÓBKI PLASTYCZNEJ METALI

S t r e s z c z e n i e

Numeryczne symulacje procesów przeróbki plastycznej wymagają dużej mocy komputerów oraz zaawansowanego oprogramowania. Uwzględnienie w analizie dużych przemieszczeń jest wielokrotnie źródłem poważnych trudności dotyczących zbieżności obliczeń. W przypadku sformułowania Lagrange'a stosowanego standardowo w analizie odkształcalnych ciał stałych często konieczne jest generowanie zupełnie nowej siatki MES, tzw. remeshingu. Wydłuża to niestety czas analizy i pogarsza jej zbieżność. W takich przypadkach rozsądną alternatywą jest zastosowanie podejścia Eulera (typowego dla analizy przepływu płynów) do obliczeń dużych deformacji ciał stałych. W podejściu Eulera siatka elementów skończonych pozostaje nieruchoma, a przez siatkę przepływa materiał. W tym przypadku nie zachodzi konieczność remeshingu i nie pogarsza się uwarunkowanie problemu w czasie trwania obliczeń. W niniejszej pracy przedstawiono przykładowe wyniki obliczeń numerycznych z zastosowaniem sprzężonego podejścia Eulera-Lagrange'a. Jako zadanie testowe analizowano belkę zginaną, jako przykład procesu przeróbki plastycznej rozpatrywano zagadnienie wyciskania przeciwbieżnego. Dla niektórych części modeli (narzędzia) stosowano sformułowanie Lagrange'a, a dla pozostałych części (obrabiany materiał) – sformułowanie Eulera. Uzyskane rezultaty porównywano z wynikami obliczeń, w których zastosowano podejście „czysto" Lagrange'owskie.

Słowa kluczowe: sprzężona analiza Eulera-Lagrange'a, duże przemieszczenia, kształtowanie plastyczne metali

DOI: 10.7862/rm.2012.9

ZESZYTY NAUKOWE POLITECHNIKI RZESZOWSKIEJ **Nr 284**
Mechanika z. 84 (4/12) **2012**

Ján SLOTA
Miroslav JURČIŠIN
Technical University of Košice, Slovakia

EXPERIMENTAL AND NUMERICAL ANALYSIS OF THE DEEP DRAWING PROCESS USING OPTICAL MEASURING SYSTEM

In this paper optimization of the deep drawing process with using a modern photogrammetric measurement system is discussed. The results obtained from optical measuring are compared with the results of a numerical simulation. The numerical simulation of this process was performed using two commercial FEM codes, which use different time integration schemes. Various results are illustrated in the details, compared and discussed. Optimization of the deep drawing process can reduce the amount of product defects, production cost and can improve the quality of products.

Keywords: deep drawing, numerical simulation, photogrammetric measurement system

1. Introduction

The deep drawing process is nowadays frequently used manufacturing technology in the industrial sphere. Many factors influence on a procedure of the forming process. These factors include for example the holding force [1, 2]. In order to optimize this process, numbers of tests have to be done. Their results may predict problematic or critical areas of the final product. Due to this in the industrial practice, numerical simulations are often used and they are based on finite element method (FEM) analysis and different time integration schemes. The most known integration schemes are the static implicit and the dynamic explicit. There are many publications which claim that only the dynamic explicit time integration scheme is accurate [3-5] or only the static implicit scheme is accurate enough [6-8]. In explicit strategy the current time step is solved once, resulting from previous time step. Based on required accuracy a mesh is locally redefined and changed. The problem is not solved again, and the solving process is not iterated. The method is convenient for tasks where the solution does not change in time [9]. Implicit strategy is in every time step starting from the previous time step and the mesh is generated using local refinement due to requiring

accuracy of the problem, which is calculated on the current mesh. This solving process is iterated until the estimated error is between the bounds of an interval and requiring precision. If the time step between a new iteration is not too large, the time of the solving process is usually very small [9]. The results of the numerical simulation may be compared with the ARGUS photogrammetric measuring system. The ARGUS is the contactless measuring system that on the basis of optical scanning allows predicting critical areas which take place during the forming process. On the sheet metal, a grid of circle points is etched before forming. The size of these points is between 1 and 6 mm. The grid is deformed at the same time as the sheet metal is deformed. The grid of circle points is deformed by the influence of direction and intensity of stresses, and its shape is changed. The measurement depends on the photogrammetric principle where the surface of a stamped part is scanned using a CCD camera in high resolution. Pictures are taken from different angles, and 3D coordinates of grid points are computed using image processing. Distances between points of the grid are defined by lateral distortion. On the basis of law of volume preservation distributions of major and minor strains, thickness reduction or critical areas of the drawn part are computed. Based on the defined material, forming limit diagram (FLD) is plotted [10]. After all points are recognized, the 3D model of the drawn part is rendered, and analysis of strains, stresses, the thickness over a section can be performed. There are several studies which dealt with the similar problems [11, 12]. The material of a blank defined in the numerical simulation was in the case of a yield function approximated using Hill 48 yield function which is defined by the following law [13, 14]:

$$\varphi\left(\sigma_{ij}\right) = F\left(\sigma_{22}-\sigma_{33}\right)^2 + G\left(\sigma_{33}-\sigma_{11}\right)^2 + H\left(\sigma_{11}-\sigma_{22}\right)^2 + \\ + 2L\sigma_{23}^2 + 2M\sigma_{31}^2 + 2N\sigma_{12}^2 - \bar{\sigma}^2 = 0 \tag{1}$$

where: $\Phi(\sigma_{ij})$ – stress components with respect to the coordinate system,
F, G, H, L, M, N – Hill's anisotropic parameters, which can be expressed by a normal anisotropy,
σ_{22}, σ_{33}, σ_{11}, σ_{23}, σ_{31}, σ_{12} – plane stresses; suffix 1 is parallel to the rolling direction, 2 is parallel to the transverse direction,
$\bar{\sigma}$ – scaling factor.

$$F = \frac{r_0}{r_{90}\left(r_0+1\right)},\ G = \frac{1}{r_0+1},\ H = \frac{r_0}{r_0+1},\ N = \frac{\left(r_0+r_{90}\right)\left(1+2r_{45}\right)}{2r_{90}\left(1+r_0\right)} \tag{2}$$

where: r_0, r_{45}, r_{90} – values of the normal anisotropy measured in directions 0°, 45° and 90° respectively to the rolling direction,
L, M – coefficients which are equal to the N.

A hardening curve was defined by values obtained experimentally and subsequently approximated with the Hockett-Sherby material model [15].

2. Objectives and approach

The aim of the experiment was to carry out the simulation of the deep drawing process in the explicit and implicit commercial software and then the results are compared with the real shape of a target product measured using the ARGUS optical measuring system. Mechanical properties of the mild steel DC05 are shown in the Table 1 and the target shape and the picture taken from the ARGUS measuring process are shown in the Fig. 1. The thickness of the blank was 0.8 mm.

Table 1. Mechanical properties of the mild steel DC05

Specimen orientation	$R_{p0.2}$ **[MPa]**	R_m **[MPa]**	A_{80} **[%]**	n	C **[MPa]**	r
0°	145	292	50.8	0.254	538.5	1.888
45°	151	298	47.9			1.464
90°	149	290	48.0			2.193

where: $R_{p0.2}$ – yield stress, R_m – ultimate strength, A_{80} – total elongation,
n – strain hardening exponent, C – strain coefficient, r – normal anisotropy

a) b)

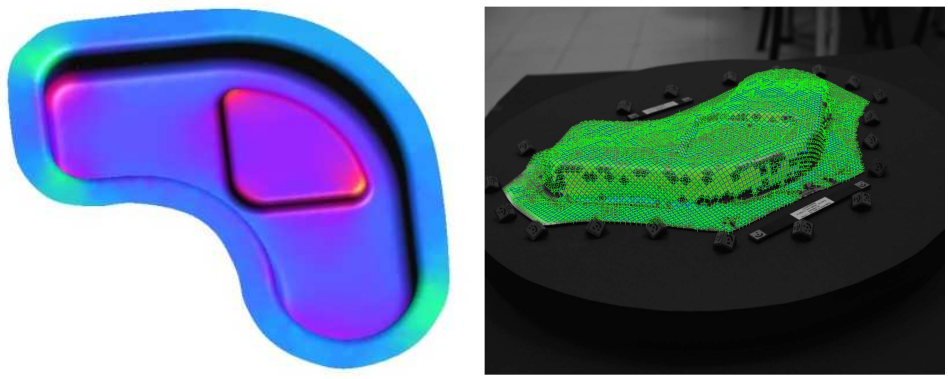

Fig. 1. Shape of the drawn part in FEM code (a) and measured in ARGUS system (b)

The punch, die and blankholder shown in the Fig. 2 were modeled in the CAD software and exported to each of FEM code. Simulation was performed in the Autoform and PAM-STAMP code. A shell element type with a different number of integration points was used. In the case of the explicit code the number of integration points was 5, and 11 in case of the implicit code. The implicit code uses a triangular mesh type with angles of 30°, and explicit code uses a rectangular mesh type with the size of 9.7 mm. The size of the element after refinement was equal to 1.2 mm. Stages defined in both FEM codes are shown in the Table 2.

Table 2. Stages defined in the implicit and explicit code

No	Stage/Code	Implicit	Explicit
1	Positioning	yes	yes
2	Holding	yes	yes
3	Drawing	yes	yes
4	Springback	yes	yes
5	Cutting	yes	no

The measurement of deformations, thickness reduction and 3D shape by the ARGUS optical measuring system was performed in the way as it was described in the previous chapter. Distances between centers of circles on the grid etched on the sheet were 1.5 mm. The results of the numerical simulation and the ARGUS measuring system will be described in the following chapter.

a) b)

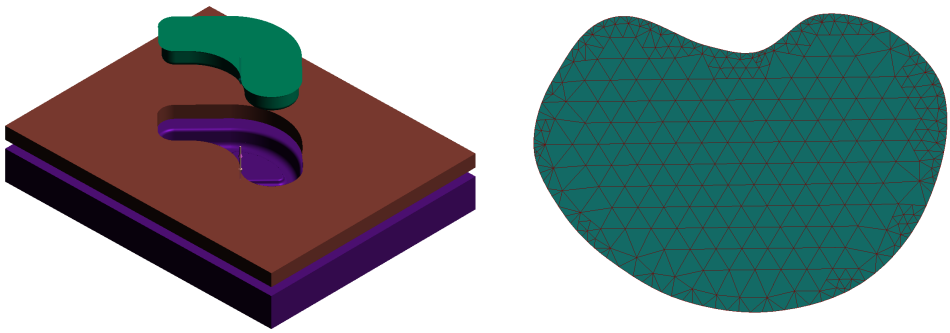

Fig. 2. Assembly of tools in the FEM code (a) and the triangular refinement of the blank (b)

3. Results of experiment

In order to compare differences between the results obtained from the ARGUS measuring system and numerical simulation, SVIEW software was

used. This comparison is necessary for interconnection of the model obtained from the FEM simulation and the model obtained from the ARGUS measuring system. All kind of inaccuracies defined in the numerical simulation can be found exactly by this comparison. The value of deviation between models is connected with the error of material model definition, the shape of tools and technological parameters defined in the numerical simulation. The deviation between models is showed in the Fig. 3.

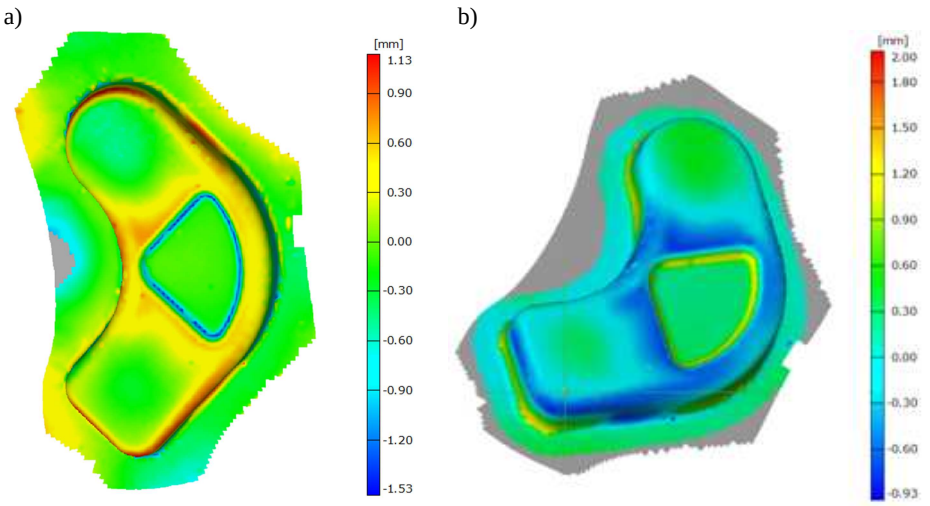

Fig. 3. Deviation of geometry of models obtained from ARGUS used explicit (a) and explicit (b) code

Hence all parameters had the same value in the case of using the explicit and implicit codes, so comparison of these solvers could be discussed. It can be seen in the Fig. 3 that both codes showed similar deviation between models, but greater geometry deviation was observed in the case of implicit solver – 2.93 mm in the absolute value. The absolute value of deviation when the explicit solver was used is 2.66 mm.

The FLD diagram of the drawn part has a key role in the assessment of the technical process suitability. The FLD diagrams exported from FEM code and the ARGUS measuring system are showed in the Fig. 4 and 5. As it can be seen, neither in FEM code, nor in the ARGUS measuring system, none point is near or over forming limit curve. The FLD diagrams were exported for the bottom membrane of the part, because by using the ARGUS measuring system it is impossible to measure deformations or to obtain FLD in neutral membrane.

Strain path of FLD is more suitable in the case of the explicit integration scheme as shown in the Fig. 5b. In the case of the ARGUS measuring system

some points in the area over 60% of major strain are visible, these points have not appeared in the FLD obtained from FEM codes.

As it was mentioned, in the ARGUS measuring system a course of thickness reduction over section can be plotted. To analyze the accuracy of FEM code in comparison to ARGUS results, analysis of the thickness reduction was performed. The section through the drawn part was showed in the Fig. 6. The reason for selecting this section was that a few critical areas are near this section. This section was defined in both FEM models and the results were compared.

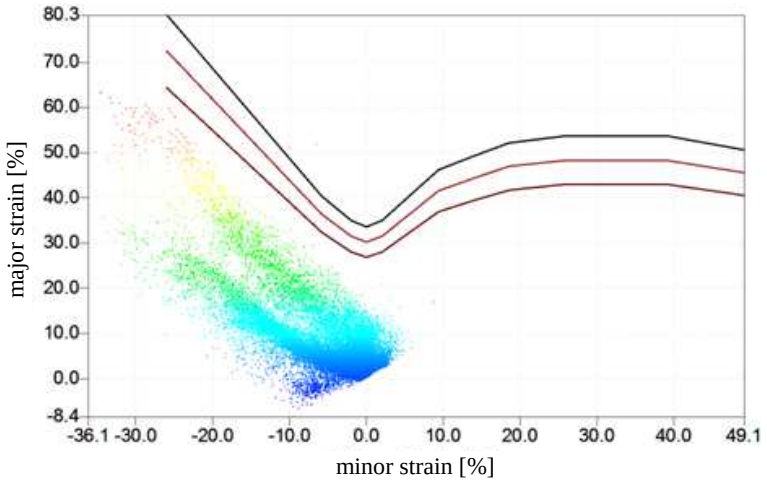

Fig. 4. FLD diagram obtained from ARGUS optical measuring system

Distribution of thickness reduction over section is showed in the Fig. 7. In this picture distribution of thickness reduction obtained from the ARGUS measuring system and FEM simulations are presented. For better understanding and orientation, section over part is represented by broken line. As it can be seen in the Fig. 7, the ARGUS, and numerical simulations recognized the problematic areas in the same places. The greatest value of thickness reduction is observed in the bottom of the drawn part. On the left radius, both – explicit and implicit codes overestimated the amount of the thickness reduction. On the right side of the drawn part, the thickness reduction was underestimated by the both FEM codes. In this case it is better to overestimate thickness reduction, because this can predict future defect. Smaller differences between numerical results and the ARGUS are observed on the right bottom radius (Fig. 7). The smallest amount of thickness reduction is observed on the bottom of the drawn part.

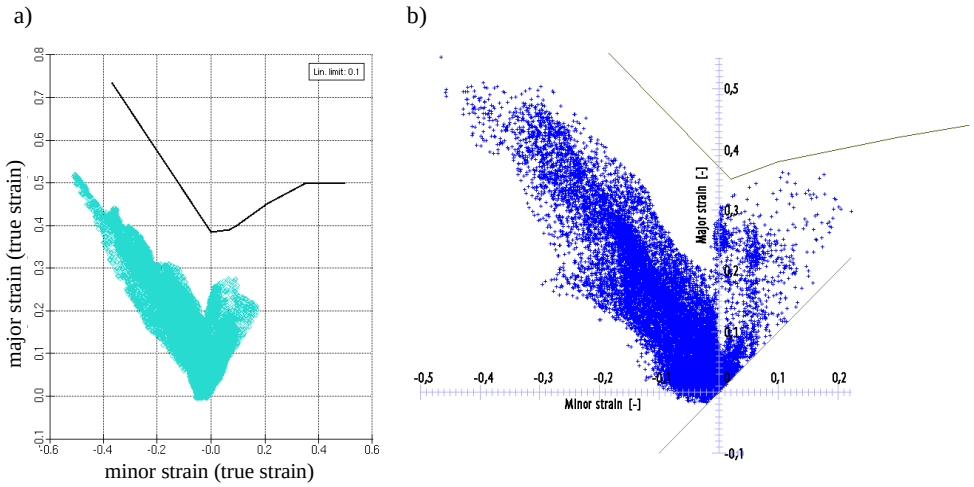

Fig. 5. FLD diagram determined using implicit (a) and explicit (b) solver

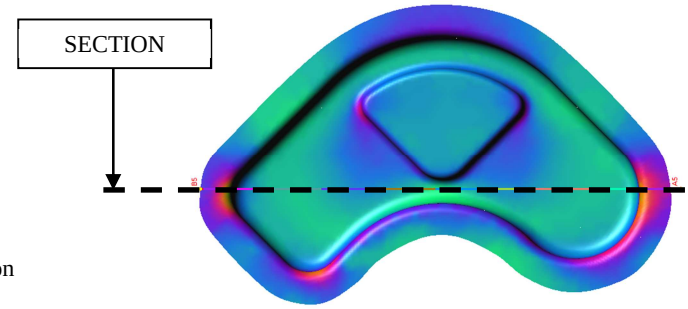

Fig. 6. Illustration of section over drawn part

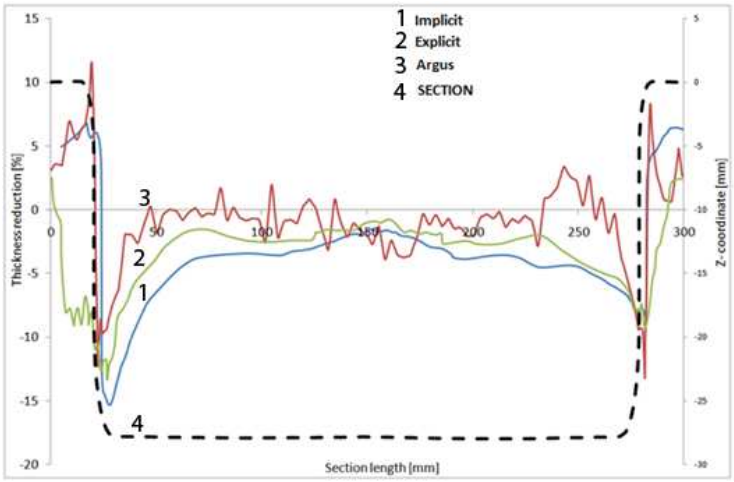

Fig. 7. Illustration of section over drawn part

4. Conclusion

Analyses of the deep drawing process using-the ARGUS optical measuring system were discussed. Simulations were carried out using two different FEM codes and verified with results of experimental measurements. It can be concluded, that both codes had approximately the same results. Using this method it is possible to verify material models used to define blank behavior. It can be concluded that the results of the numerical simulation are accurate enough to predict critical areas of the drawn part. The same critical places of the drawn part were recognized with the ARGUS measuring system and both FEM codes. In the case of the FLD diagram there were no points over the forming limit curve. Considering the fact that implicit code needs less computing time according to explicit code, and the results varied about small values, it can be concluded that the implicit code is more convenient to use. Moreover, the implicit code needs less parameters which have to be defined, and needs less time spending with definition. Using the ARGUS optical measuring system leads to prediction critical areas on the drawn part and to optimization of the whole deep drawing process.

References

[1] Ahmetoglu M., Altan T.: Deep drawing of round cups using variable blank holder force (BHF), Reoirt Bi, ERC/NSM-S, Engineering Research Centre for Net Shape Manufacturing, Ohio State University, Ohio 1992.

[2] Obermeyer E.J., Majlessi S.A.: A review of recent advances in the application of blank holder force towards improving of the forming limits of sheet metal parts, J. Mat. Proc. Technol., 75 (1998), 222-234.

[3] Lig Y., Tan M.J., Liew K.M.: Springback analysis for sheet forming processes by explicit finite element method in conjunction with the orthogonal regression analysis, Int. J. Solids and Structures, 36 (1999), 4653-4668.

[4] Yang D.Y., Jung D.W., Song I.S., Yoo D.J., Lee J.H.: Comparative investigation into implicit, explicit, and iterative implicit/explicit schemes for the simulation of sheet-metal forming processes, J. Mat. Proc. Technol., 50 (1995), 39-53.

[5] Jung D.W.: Static-explicit finite element method and its application to drawbead process with springback, J. Mat. Proc. Technol., 128, 1-3 (2002), 292-301.

[6] Meinders T. et.al.: A sensitivity analysis on the springback behavior of the unconstrained bending problem, J. Mat. Proc. Technol., 9, 3 (2006), 365-402.

[7] Li K., Geng L., Wagoner R.H.: Simulation of springback: Choice of element, [in:] Advanced technology of plasticity, M. Geiger (ed.), vol. 3, Springer-Verlag, Nuremberg 1999, 2091-2099.

[8] Hu Y.: Quasi-static finite element algorithms for sheet metal stamping springback simulation, Proc. of 4th Int. Conference and Workshop on Numerical Simulation of 3D Sheet Forming Processes, NUMISHEET 1999, J.C. Gelin and P. Picart (eds.), 71-76.

[9] Schmidt A., Kunibert G.S.: Design of adaptive finite element software. The finite element toolbox, Springer-Verlag, Bremen 2004.
[10] ARGUS USER GUIDE, http://www.gom.com/.
[11] Frącz W., Stachowicz F., Pieja T.: Aspect of verification and numerical optimization of sheet metal and numerical simulations process using the photogrammetric system, Acta Metallurgica Slovaca, 19 (2013) (in press).
[12] Solfronk P., Sobotka J.: Utilization of forming tool with variable blankholder force for drawing of al alloys, Physics Procedia, 22 (2011), 233-238.
[13] Réche J., Besson J., Sturel T., Lemoine X., Gourgues-Lorenzon A.F.: Analysis of the air-bending test using finite-element simulation: Application to steel sheets, Int. J. Mech. Sci., 57 (2012), 43-53.
[14] Roll K.: Simulation of sheet metal forming – Necessary developments in the future, Int. Conf. NUMISHEET 2008, Interlaken, Switzerland 2008, 3-11.
[15] AUTOFORM user guide, http://www.autoform.com/.

This contribution is the result of projects implementation: Center for research of control of technical, environmental and human risks for permanent development of production and products in mechanical engineering (*ITMS: 26220120060*) *supported by the R&D Operational Programme funded by the ERDF and VEGA 1/0396/11.*

ANALIZA EKSPERYMENTALNA I NUMERYCZNA PROCESU GŁĘBOKIEGO TŁOCZENIA ZA POMOCĄ OPTYCZNEGO SYSTEMU POMIAROWEGO

S t r e s z c z e n i e

Wyniki otrzymane z zastosowaniem optycznego systemu pomiarowego zostały porównane z wynikami symulacji numerycznych. W artykule przedstawiono optymalizację procesu głębokiego tłoczenia z wykorzystaniem nowoczesnego fotogrametrycznego systemu pomiarowego. Symulacja numeryczna tego procesu została wykonana za pomocą dwóch komercyjnych programów MES z użyciem różnych schematów całkowania czasu. Różne wyniki zostały szczegółowo zilustrowane, porównane i omówione. Optymalizacja procesu głębokiego tłoczenia może zmniejszyć liczbę wad wyrobu i koszt produkcji oraz poprawić jakość wyrobów.

Słowa kluczowe: głębokie tłoczenie, symulacja numeryczna, fotogrametryczny system pomiarowy

DOI: 10.7862/rm.2012.10

ZESZYTY NAUKOWE POLITECHNIKI RZESZOWSKIEJ **Nr 284**
Mechanika z. 84 (4/12) **2012**

Roman ŠÚŇ
Emil SPIŠÁK
Technical University in Košice, Slovakia

EVALUATION OF THE CUTTING EDGE FAN-SHAPED DURING THE CUTTING PROCESS BY THE HYDRO ABRASIVE WATER JET

This article presents the current state of hydro-erosion cutting and factors affecting the quality of cutting surface. The aim of this article is the evaluation of the fan-shaped water spray pattern on the bottom cut edge by the hydro-erosion cutting based on selected parameters like cutting surface roughness and the distance between the inlet and outlet water jet. The results demonstrate that cutting speed had the largest influence on evolution of fan-shaped bottom of the cut edge because increasing cutting speed increases the values of both parameters mentioned above.

Keywords: hydro-erosion cutting, cutting speed, fan-shape, cutting surface quality

1. Introduction

The cutting process of the material by the high pressure hydro abrasive water jet consists in removing a material by the mechanic effect of a narrow abrasive water jet at a high rate. The abrasive is used to increase the rate and the final quality of the cut material process [1]. High rate hydro abrasive water jet is generated by means of a hydraulic pump creating high pressure water that is by means of 0.1-0.3 mm diameter water jet cutter transformed into high rate water. The water jet penetrates the workpiece, gradually loses its kinetic energy and skews [2]. The place where the water jet comes into contact with the cut material, gives rise to the reduction of the cut material by the controlled process. The result of such a process is a continuously cut material. Regarding the fact that a cut material is predominantly an abrasive with water, in the place where the material is cut, traces of the water jet effect in the cut direction and movement are visible. These traces of the water jet effect can be eliminated or even removed by the change of cutting parameters. Quality degrees of the surface topography introduced by KMT firm are also used in this article and are stated in five categories (Table 1).

Table 1. Quality degrees of the surface topography

Degree	Characteristic	Roughness Ra_{HK} [μm]	Roughness Ra_{DK} [μm]
Q1	dividing cut	4.0-6.3	≤ 40
Q2	rough cut	≤ 4.0	≤ 25
Q3	middle cut	≤ 4.0	≤ 12.5
Q4	quality cut	≤ 3.2	≤ 6.3
Q5	best cut	< 3.2	≤ 3.2

Ra_{HK} – roughness in the top outline, Ra_{DK} – roughness in the bottom outline

Factors characterising the surface created by hydro erosion (surface of the cut edge) in relation to the quality and productivity hydro erosion process are stated in three categories [3]:

1) basic physical properties,
2) the technical factors influence effecting the hydro erosion process,
3) the technological factors influence on the hydro abrasive surface erosion.

Analysis of these factors and dimensioning of their optimal setting have an important influence on the quality of the operation of the technological process and the surface made by hydro erosion. During the process of material cutting by the high rate hydro abrasive water jet, the form of the device – water jet is changed [4]. At a distance of entering the water jet the cut material, the diameter of the water jet is expanded and diverted from the originally perpendicular water jet from its own axle. The size of the shape change that can be called curvature primarily depends on the rate of the device movement and the thickness and mechanical properties of the cut material. Energy decrease, resistance of the cut material and the movement rate are the basic factors affecting the characteristic shape of the device (water jet) in the cutting material [5, 6].

The curvature of the water jet is made in the opposite direction in comparison to the movement of the cutting head. The increasing of the deflection angle of the leaving water jet against the entering water jet is manifested in the worsening of surface quality that is expressed in the roughness of a new made surface and perpendicularity deflection of the material cut edge in the perpendicular direction to the cutting direction. Position of the place where the water jet enters the processed material is not compatible with the place where the water jet leaves the material. The place of the leaving water jet lags the place of the entering water jet. The lagging of the lower part of the water jet in comparison to the upper part is designated as „jet lag“; in the picture below (Fig. 1) designated as „L“. The size of the jet lag is in the region of tenth millimetre up to several dozen millimetres and is a natural sign of an economical cutting way [7, 8].

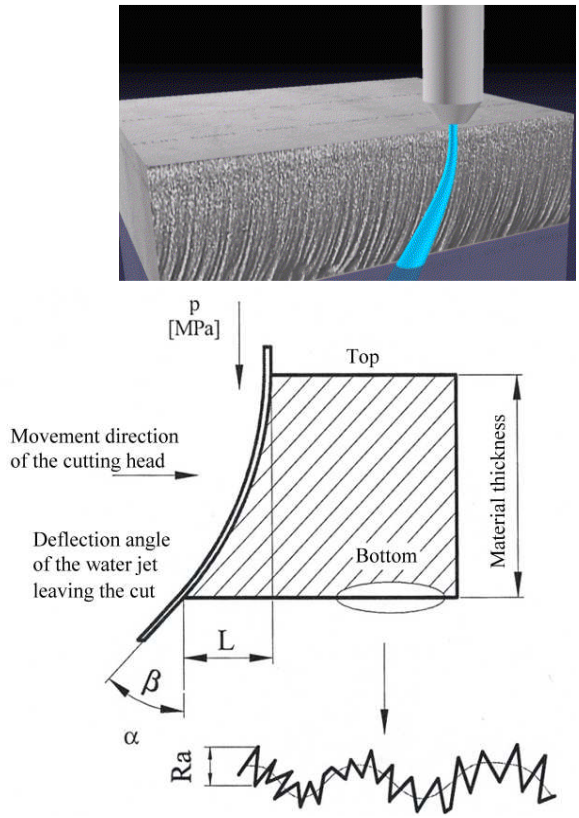

Fig. 1. Trace deflection of cut flag

2. Material and testing

In our research, test samples of stainless material STN 41 7240, class 17 240 – AISI 304 were used. This material represents chromium-nickel steel and, as to the anti-corrosive materials, it is the second most frequently used kind of material thanks to its resistance to corrosion, its cold forming and good welding property. The chromium-nickel steel is resistant to water, humidity, edible acids and weaker organic and anorganic acids. Temperature strain of this steel amounts to 300°C. AISI 304 is well publishable and suitable to be used in operations of deep drawing, folding and curling. This material is also suitable for electric arc but unsuitable for blaze welding. Test samples with a depth of 15 mm were cut by the abrasive water jet device with a high pressure pump SL II 50K and two CNC X-Y tables of 3000 x 1500 mm, next AUTOLINE I cutting head and an abrasive (Bengal Bay Garnet). The other constants and parameters are stated in the tables. Test samples were cut in four phases:

- perforation of the sample,
- 10 mm length cut from the perforation point (for the measurement of the cut boundary),
- sample cutting in the shape of a square (sides marked as *a*, *b*, *c*, *d*),
- each edge is cut at a different rate (a = 50 mm/min, b = 75 mm/min, c = 100 mm/min, d = 125 mm/min.

Samples were cut altogether and all diameters were written down into a collecting register of test samples cutting. 16 samples out of the total amount of 64 have been selected for the purposes of this study. The results of measuring and cutting have been recorded in the tables and evaluated with the help of graphs. For the evaluation of the fan-shaped of the cut edge by the hydro erosion, roughness measurements of the cut edge of samples and measurements of size distance between water jet entering and water jet leaving were carried out as representing parameters influencing the creation of the fan-shaped of the lower cut edge of the cut material. The following parameters have remained constant with each tested sample:

- abrasive – Bengal Bay Garnet (Mesh 80),
- water pressure – 300 MPa,
- abrasive jet – ø 1.02 mm.

With regard to the extensiveness of the experiment, not all factors are stated; not all factor influencing the final quality of the cut surface as well as other evaluated parameters such as edge fanshaped and cut depth. Selected samples have been divided into 4 groups, each group containing 4 samples:

Group 1 – amount of abrasive 100 g/min; distance of water jet from material is 5 mm.

Group 2 – amount of abrasive 150 g/min; distance of water jet from material is 3 mm.

Group 3 – amount of abrasive 200 g/min; distance of water jet from material is 3 mm.

Group 4 – amount of abrasive 250 g/min; distance of jet from material is 3 mm.

The following parameters have remained constant with each tested sample:

- abrasive – Bengal Bay Garnet (Mesh 80),
- water pressure – 300 MPa,
- abrasive jet – ø 1.02 mm.

With regard to the extensiveness of the experiment, not all factors are stated; not all factor influencing the final quality of the cut surface as well as other evaluated parameters such as edge fan-shaped and cut depth (Figs. 2-5).

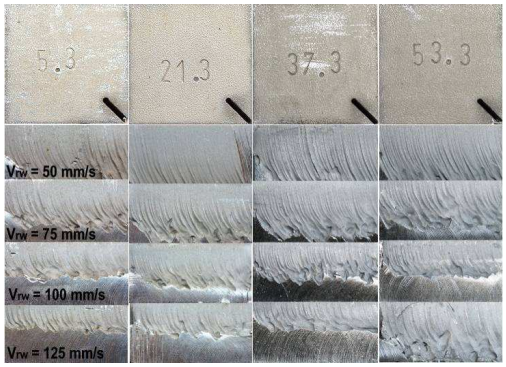

Fig. 2. Surface view of selected test samples cut with abrasive amount of 100 g/min

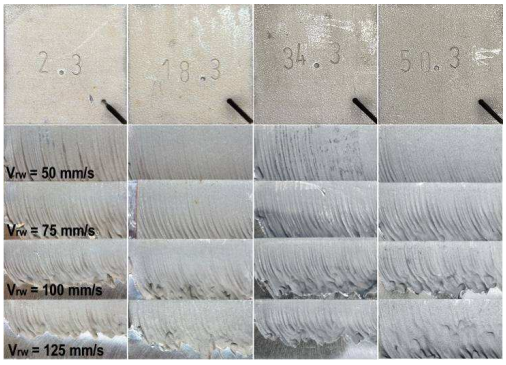

Fig. 3. Surface view of selected test samples cut with abrasive amount of 150 g/min

Fig. 4. Surface view of selected test samples cut with abrasive amount of 200 g/min

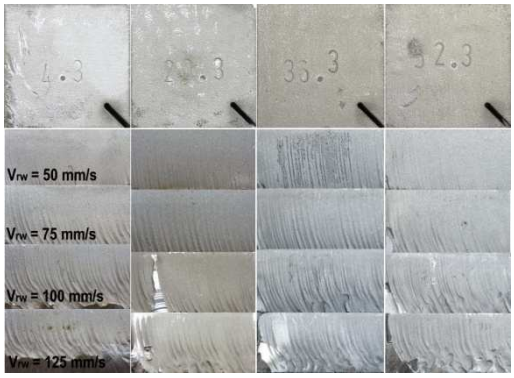

Fig. 5. Surface view of selected test samples cut with abrasive amount of 250 g/min

3. Evaluation of the cutting edge fan-shaped

A digital calliper Powerfix Profi has been used to measure and evaluate the intruded length of jet. The sample has been optically evaluated and the distance has been measured, by means of a calliper, in the most accentuated place of water jet entering and leaving (Fig. 6). The values gained have been written down into tables and evaluated by means of graphs (Figs. 7-10).

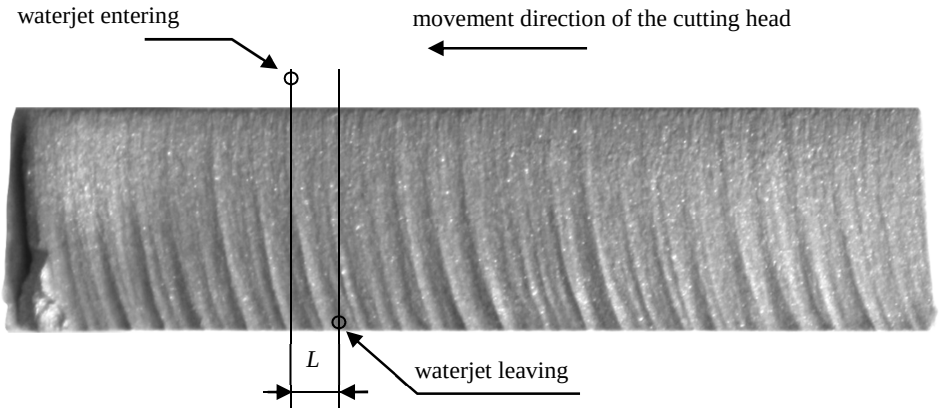

Fig. 6. Distance measurement between water jet entering and leaving

As it is shown in Fig. 7, the distance between input and output beam at a constant amount of abrasive 100 g/min decreased with increasing cutting speed. This graph clearly shows that the cutting speed of 125 mm/min is the optimum choice and cutting speed of 75 mm/min is the worst possible because featheriness is the greatest. Next graph (Fig. 8) shows that a constant amount of abrasive at 150 g/min, the distance between the input beam and output beam

appears as the best possible in cutting speed of 50 mm/min and the worst possible choice would be to use a cutting speed of 100 mm/min, because the featheriness is the largest. Graphic evaluation of a constant amount of abrasive of 200 g/min (Fig. 9) clearly shows that the best used cutting speed appears cutting speed of 50 mm/min, where the distance between input and output beam is minimum. Opposite, proportionally increasing of featheriness using higher cutting speeds, that the highest cutting speed, 125 mm/min seems like the worst possible because featheriness is the greatest. As in the previous graph, graphical evaluation at a constant amount of abrasive 250 g/min (Fig. 10) shows that the increasing proportion of featheriness is based on increasing speed. We can conclude that for this quantity of abrasives, the most appropriate cutting speed seems to be 50 mm/min and as the worst possible speed is 125 mm/min due to featheriness.

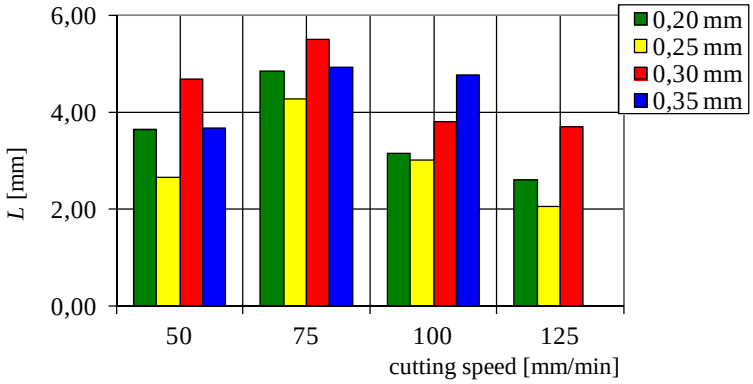

Fig. 7. The distance between water jet entering and leaving *L* dependence on cutting speed and water jet diameter, with abrasive amount of 100 g/min

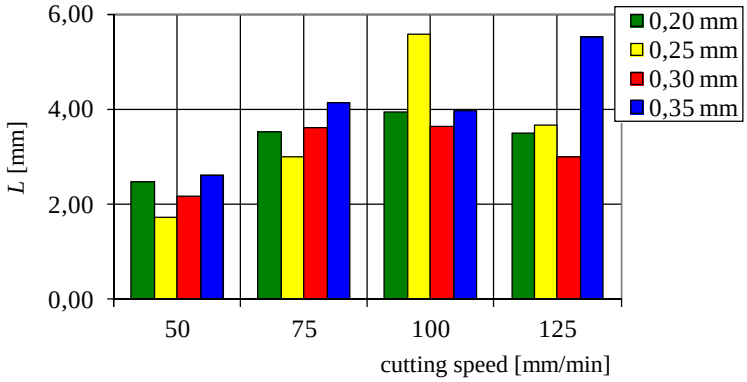

Fig. 8. The distance between water jet entering and leaving *L* dependence on cutting speed and water jet diameter, with abrasive amount of 150 g/min

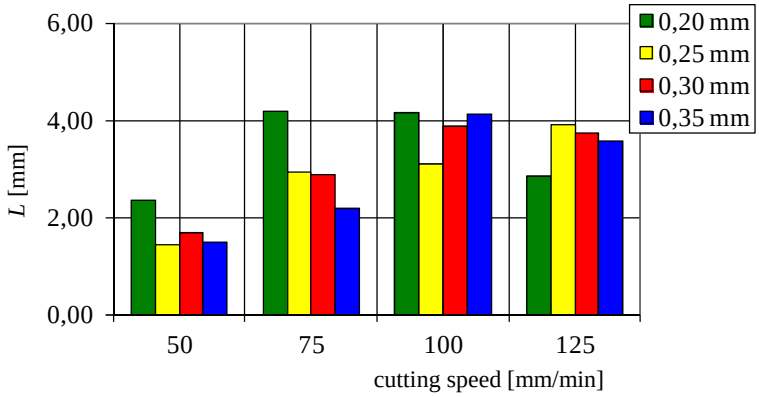

Fig. 9. The distance between water jet entering and leaving *L* dependence on cutting speed and water jet diameter, with abrasive amount of 200 g/min

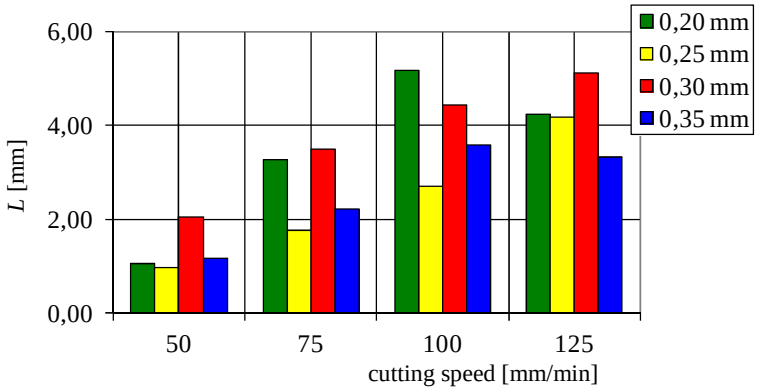

Fig. 10. The distance between water jet entering and leaving *L* dependence on cutting speed and water jet diameter, with abrasive amount of 250 g/min

4. Evaluation of the cutting edge roughness

Roughness measuring was realized by Mitutoyo SJ-301 roughness measurement. The middle value was evaluated for *Ra* roughness for each side of evaluated samples. Roughness was evaluated with follow results:

1. At constant amount of grit 100 g/min, machined surface roughness has increased with increasing cutting speed (Fig. 11). At a cutting speed of 50 mm/min roughness was soft and at a cutting speed of 125 mm/min the roughness was harder. Finally we can conclude that this is maximum cut because the minimum value of Ra was 6.3 μm.
2. The Figure 12 shows that a constant amount of grit 150 g/min used at low speeds it seems to have positive effect on the soft roughness. Conversely,

once again it confirmed that the rising rate negatively affects the roughness. We can conclude that this is maximum cut because the minimum value of *Ra* was 6.3 μm.

3. Using a constant amount grit 200 g/min, that for a given amount of abrasive there is a significant difference in roughness between the lowest and highest cutting speed (Fig. 13). Again, cutting speed of 50 mm/min appeared to be optimal and cutting speed 125 mm/min appeared as inappropriate. We can conclude that this is maximum cut, because of the smallest value of *Ra* that is in the range 4.0 to 6.3 μm.
4. The Figure 14 clearly shows that a constant amount of abrasives 250 g/min appears again the lowest cutting speed 50 mm/min is optimal and cutting speed 125 mm/min as inappropriate. The highest values of the roughness but not as high as in the previous figures, when a smaller amount of abrasives was used. Nevertheless, we can conclude that this is maximum cut because the lowest value of *Ra* is in the range of 4.0 to 6.3 μm.

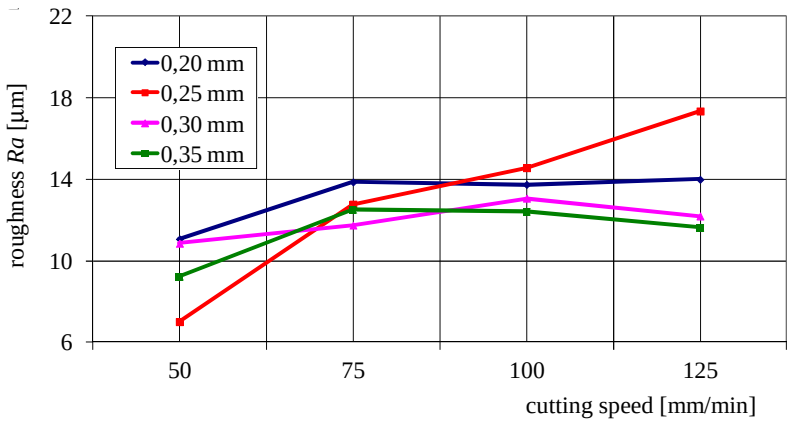

Fig. 11. The cutting edge roughness dependence on cutting speed and water jet diameter, at constant average abrasive nozzle ø1.02 mm, distance of nozzle from material 5 mm, abrasive quantity of 100 g/min

Based on the evaluated results, it was found that the positive effect on the quality of the cutting edge has lower cutting speed and more abrasive. At a cutting speed of 50 mm/min abrasives and weights of 200 g/min, the roughness ranged from 5.69 to 8.82 microns, which appeared to be optimal ratio selected. Negative impact on the quality of the cutting edge is a cutting speed, 100 mm/min and 125 mm/min. Surface roughness at a cutting speed of 125 g/min abrasives and weights 150 g/min ranged between 18.2 to 21.21 μm.

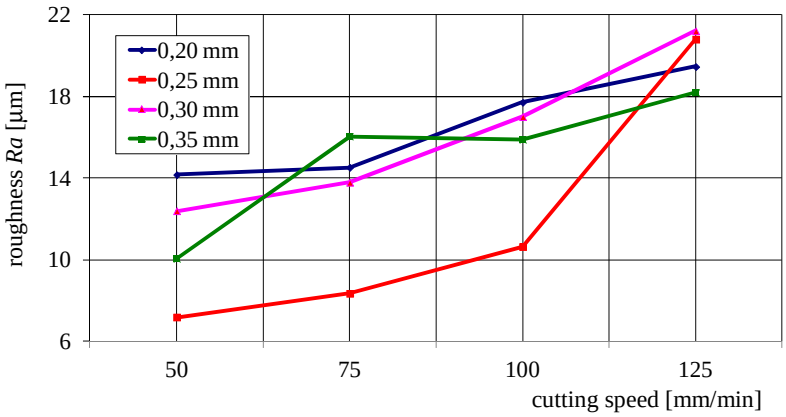

Fig. 12. The cutting edge roughness dependence on cutting speed and water jet diameter, at constant average abrasive nozzle ø 1.02 mm, distance of nozzle from material 3 mm, abrasive quantity of 150 g/min

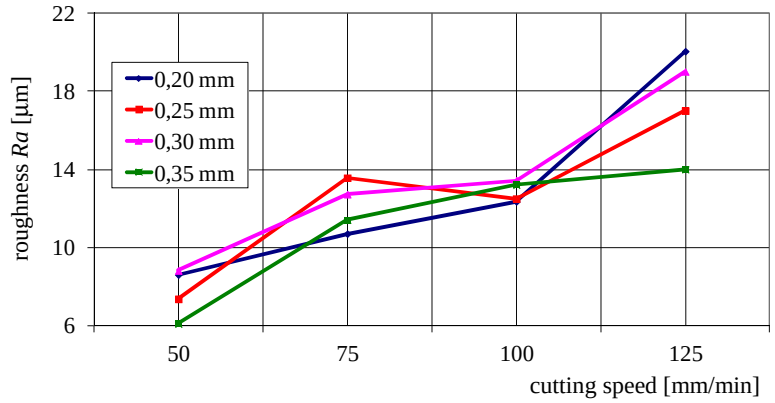

Fig. 13. The cutting edge roughness dependence on cutting speed and water jet diameter, at constant average abrasive nozzle ø 1.02 mm, distance of nozzle from material 3 mm, abrasive quantity of 200 g/min

5. Conclusion

Based on the evaluated results, it has been determined that the distance between water jet entering and water jet leaving decreased with the increasing abrasive amount and by following lower cutting rates. The increasing of a cutting rate negatively influences on the quality of the cut surface and the distance between water jet entering and water jet leaving, because the increasing of

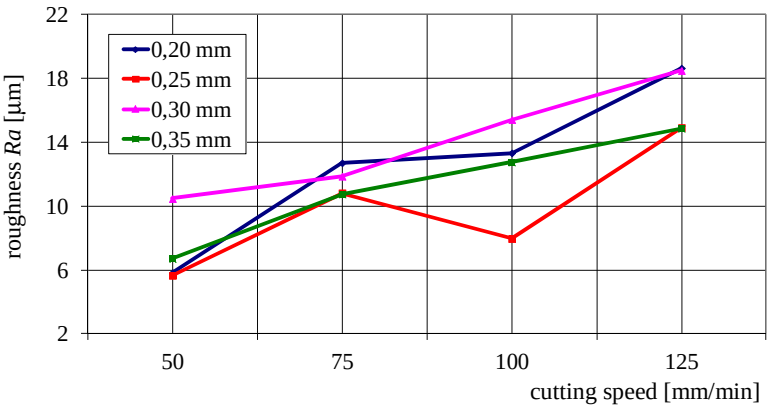

Fig. 14. The cutting edge roughness dependence on cutting speed and water jet diameter, at constant average abrasive nozzle ø 1.02 mm, distance of nozzle from material 3 mm, abrasive quantity of 250 g/min

a cutting rate increases also values of the mentioned parameters. As to the distance between water jet entering and water leaving, the abrasive amount of 200-250 g/min at the rate of 50 mm/min is considered to be optimal, but outside this range the influence of the abrasive amount impacts negatively, primarily on water jet entering and water jet leaving that has a direct influence on the cut edge fan-shaped. As an acceptable fan-shaped is considered the one visible to the naked eye because the bottom edge of the cut surface is no more relatively straight then.

References

[1] Maňková I.: Progresívne technológie: Advanced methods of material removal, Vienala, Košice 1999.
[2] Híreš O., Hatala M., Hloch S.: Delenie kovových materiálov okružnou pílou, vodným prúdom a plazmovým oblúkom, JIŘÍ PUSTINA, Ostrava 2007.
[3] Kmec J.: Vplyv parametrov vodného lúča na povrch vytvorený hydroabrazívnou eróziou, Vienala, Košice 2010.
[4] Sobotová L., Tkáčová J.: Progresívne technológie. Návody na cvičenia, TU, SjF, Košice 2008.
[5] Wilkins R.J., Graham E.E.: An erosion model of waterjet cutting, ASME J. Engng. Industry, 115 (1993), 57-61.
[6] Fabianová J.: Význam skúmania vplyvu rezných parametrov pri rezaní vodným lúčom, Výrobné Inžinierstvo, 2 (2007), 53-55 (online: http://web.tuke.sk/fvtpo/ /journal/pdf07/2-str-53-55).
[7] Vasilko K., Kmec J.: Delenie materiálu, DATAPRESS, Prešov 2003.
[8] Waterjet machining tolerances: Limits to tolerance (online: http://waterjets.org/ /index.php?option=com_content&task=view&id=185&Itemid=54).

OCENA WACHLARZOWATOŚCI KRAWĘDZI CIĘCIA PODCZAS PROCESU CIĘCIA STRUMIENIEM WODNO-ŚCIERNYM

S t r e s z c z e n i e

Artykuł przedstawia bieżący stan wiedzy na temat erozyjnego cięcia strumieniem wody oraz prezentuje wskaźniki, które wpływają na jakość powierzchni przecięcia. Celem artykułu jest ocena wachlarzowatości dolnej krawędzi powierzchni przecięcia na podstawie wybranych parametrów, takich jak chropowatość powierzchni przecięcia i odległość pomiędzy wlotem i wylotem strumienia wody. Wyniki badań wskazują, że prędkość cięcia ma największy wpływ na rozwój wachlarzowatości dolnej krawędzi powierzchni przecięcia, ponieważ zwiększenie prędkości cięcia zwiększa wartość obu wymienionych parametrów.

Słowa kluczowe: cięcie wodno-erozyjne, prędkość cięcia, wachlarzowatość, jakość powierzchni cięcia

DOI: 10.7862/rm.2012.11

ZESZYTY NAUKOWE POLITECHNIKI RZESZOWSKIEJ **Nr 284**
Mechanika z. 84 (4/12) **2012**

Tomasz TRZEPIECIŃSKI
Rzeszow University of Technology

ADVANCES IN SHEET METAL FORMING TECHNOLOGIES

In the article the changes associated with construction of machines used in die and die-less sheet metal forming have been presented. The selected future directions of development in new technologies and machines for sheet metal forming taking into account modern blank holding systems in the process of deep drawing have been indicated. Also the tendencies in introduction of new technologies and modernization of presently used technologies in order to increase productivity have been discussed.

Keywords: blankholder, blankholder system, deep drawing, sheet metal forming

1. Introduction

The development of power transmission systems of modern machines results in replacement of mechanical drives by hydrostatic, electrical and hybrid drives. The control of technological machines for metal forming is based on computer numerical control (CNC) systems and programmable logic controllers (PLC) as well as digital linear actuators. Mechanical transport mechanisms are replaced by robots and manipulators with higher adaptivity. Together with development of hydraulic and pneumatic drives, servo drives and digital linear drives it is possible to optimize the operating space of machines and to decrease the material consumption index. The most important characteristics of CNC machines used in sheet metal forming compared to the conventional machines are:

- automatic control systems feedback with control computer,
- many axes numerically controlled,
- application of automatic tool changer systems and 3-axis automatic modular transport systems,
- automatic diagnostic systems of collision and errors of primary control program,
- application of servo drives and precise toothed bars allowing to minimize clearances.

Introducing into the market new constructional solutions of machines is connected with analysis of raising expectation of dimensional accuracy of products, processing speed, forming forces as well as static and dynamic rigidity [1]. Analysing the machine market over last few years it can be observed, that producers are concentrated on elastic adaptation of machines for industrial consumer needs [2].

2. Deep drawing

The development of sheet metal forming presses is connected with growing requirements of automotive industry and is focused on improvement of material flow and modernization of press driver. Increasing of material flow rat is realized by connection of press lines by using robots and 3-axis transfer machines with modular transport systems [3]. Presently used autogenous press lines are composed with autonomous systems of material supply, manipulation and transport of finished products [4]. The CNC controlling in hydraulically driver forming presses enables regulation of forming force and speed of press ram in the whole range of slide motion. The servo drive of crank presses allows for selection of drawing characteristics with codominant lower energy-consumption compared to the classical drives.

The introducing into the market servomotors coupled with programmable PLC controllers by SEYI enables modification of stamping process characteristics and it is possible to set up low rotational speed of crankshaft. The example of usage direct servo drive press SD series is pressing with programmable pulsating motion that reduces undesirable residual stresses in a drawpiece [5, 6]. The innovative compact design of the press frame is combined with its own motor design – specially developed, low speed servomotor with high torque and low energy consumption. Combined with an easy-to-operate, free programmable control system, it is possible to achieve dramatically reduced power consumption, improve productivity and extend tool life by 5-10 times.

Progress in sheet metal forming technology is also connected with development of new techniques and machines for sheet metal cutting [7]. Modernization of sheet-metal forming presses is connected not only with development of traditional stamping methods but also there is the extensive growth of new machines using a multi-segmented flat and tapered blankholders [8], pulsatory and elastic blankholders [9], intelligent multi input multi output (MIMO) systems with numerically controlled blankholder force (BHF) [10, 11].

3. Progress in blankholder systems

In the pulsating blankholder system the blankholder is subjected to a vibratory (pulsating) force. The metal flowing into the bottom die is subjected to intermittent pressure at a frequency of up to 20 Hz. The material flow much better under the blankholder without the disadvantages of an essential low hold-down force. Increase of pulsation amplitude of the blank holder leads to decrease of frictional resistance and has a decisive effect on drawpiece quality [12]. Some researches [13, 14] concluded that the increase of the frequency of the vibration leads to increase in the drawability and also results in a general decrease in thinning in comparison to the constant BHF. A pulsatory blankholder scheme could lead to reduction of the friction forces between the blankholder and blank, without increasing the danger of wrinkling and rapture [15]. The newest tendencies to minimize the punch force and increase in limiting draw ratios affected the development of friction-actuated blank-holding technique [16] and elastic (pliable) blankholders [17]. Blank holding is induced by applying a pressure on the upper surface of the elastic ring plate, which upon deflection would conform to the flange surface [12]. Application of elastically deformable thin plate instead of classical rigid blankholder aims at enhancing more uniform contact conditions nearly all over the flange zone in contrast to the contact at the outer rim of the flange which is dominant in the case of the conventional rigid blankholder. Present effort is made to develop effective optimization techniques and devices to control process parameters and optimize the blankholder schemes. Based on the punchless deep drawing process [18] a new eight segments flat blankholder device was proposed [19]. This device is made by fitting four flat small wedges in the gaps between the four flat drawing segments. In the case of forming thin sheets, a crack was observed due to the localized intensive shear deformation at the boundaries between the drawing segments and the wedges. To eliminate this defect a friction aided deep drawing process using tapered blankholder divided into four segments was proposed [20]. The blankholder is made by cutting a tapered steel blankholder into eight segments. It consists of a stationary base and eight tapered drawing segments that have similar planes of 5° taper angle (Fig. 1c). The drawing segments can slide in radial direction under a constant speed over the tapered surfaces of the stationary base. In the first drawing step, deformation starts when four facing segments move radially inward to the die opening in the A-direction as shown in Fig. 1a. The other four segments in the B-direction move in the reverse direction, i.e. downward and radial outward opposite to the drawing direction as shown in Fig. 1b. In the A-direction the blank sheet and the die are lifted up (Fig. 1b), while in the B-direction there is no contact between the sheet and segments (Fig. 1c).

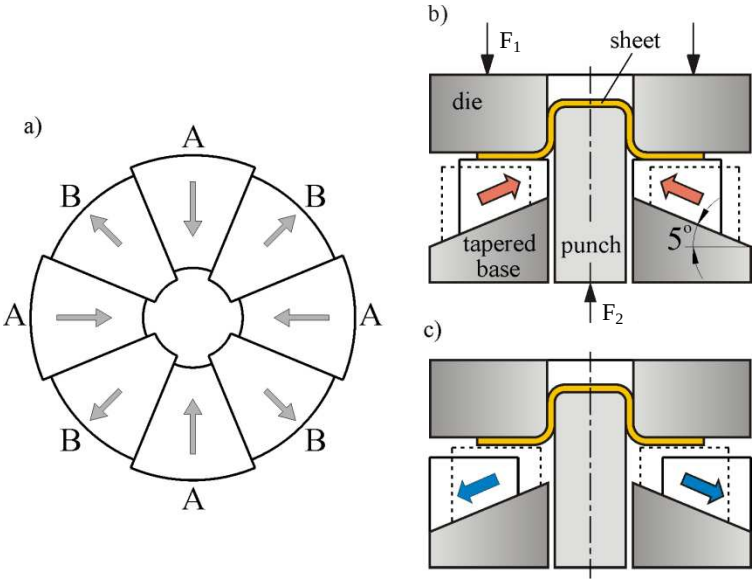

Fig. 1. Schematic of eight segments tapered blankholder (a) and schematic of die in motion (b, c)

The flexible manufacturing system using multi-point forming (MPF) technology is an advanced digital tooling system for the automatic fabrication of 3D surface parts [21]. The main characteristic of the deformation method is given by the active surface discrete design of the forming elements which are composed of a number of pins, vertically aligned, according with the geometry of the part [22]. The surface tooling in reconfigurable multipoint forming (RMF) is based on the concept of a die continuous surface discrete approximation (Fig. 2a). Usage of multi-point dies (Fig. 2b) mounted on special multipoint press machine (Fig. 2c) allows to obtain drawpieces with higher shape precision and under the decreased forming force, compared to traditional deep drawing.

Based on the MPF methodology, an innovative dieless tooling (DT) and jigless tooling (JT) system is being developed. The DT/JT system integrates the technology of MPF with the technology of computer-aided and computer-controlled manufacturing.

Overcoming mass production problems following try-out, new press technologies continuously emerge as new techniques and ideas in sheet metal forming are considered in press design. Controlling the flow of sheet metal via controllable multi-cylinder blankholder actuators reduces die-try out time by cutting down on die work [23-25]. The application of multi-input multi-output (MIMO) stamping process controller especially in case of forming complex-geometry parts allows to apply the non-uniform BHF in different regions of the drawpiece [23, 26].

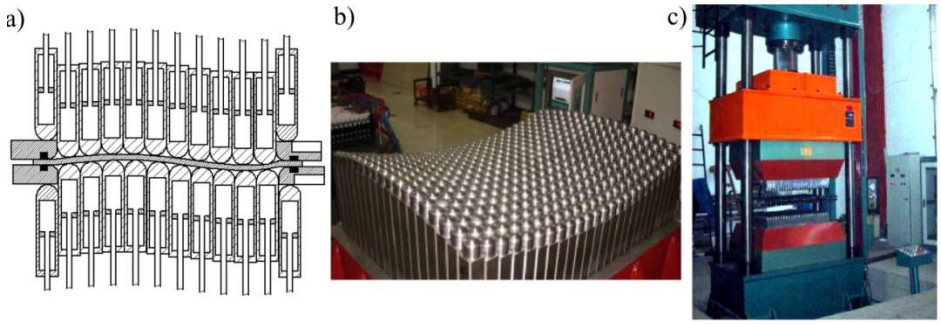

Fig. 2. Reconfigurable surface tooling (a), multi-punch stamping die (b) and multipoint forming press machine YAM8-315 (c), prepared on the basis of [21, 23]

The deep drawing processes usually were done in the double-acting presses (most often used) with two rams or in the single-acting presses with a cushion system in the press table. In some single-acting presses, hydraulic cylinders are installed at the four corner points of the press table. Each cylinder has its own proportional or servo valve so that specific BHF can be run over the stroke for each cylinder. The BHF is transmitted from the cushion plate to the blankholder by several cushion pins. Numerically controlled height-adjustable cushion pins in hydromechanical multipoint cushion system have been recently developed [27]. Each cushion pin has its own load cell to monitor the BHFs, which are introduced to the blankholder. In the flexible die blankholder system the blankholder is made from a nylon-based thermoplastic material and designed with pyramid-shaped steel inserts (Fig. 3). The BHFs are introduced into the pyramid-shaped steel inserts (top down), so there is a clear correspondence between the BHF and the pressure-influenced base area of the pyramid. Between the stiff steel inserts, the flexible plastic material acts like elastic links.

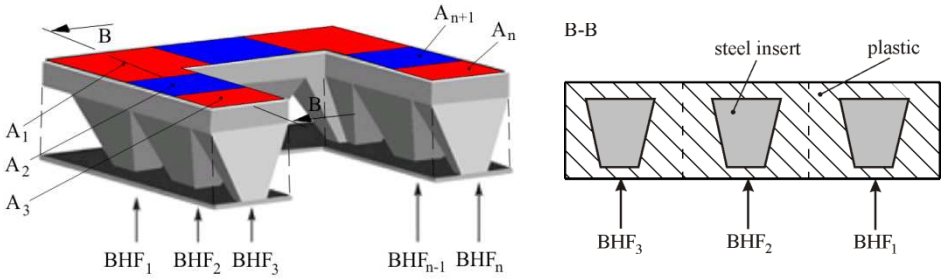

Fig. 3. Multi-point blankholder, where: A_1-A_3 – flat surfaces, BHF (1- n) blankholder forces

4. Development of other innovative processes

Development of innovative sheet metal forming technologies in last years determines progress in control systems and construction of presses and tools. Considerable growth of forming techniques may be noticed in hydroforming, electromagnetic metal forming, sheet metal forming with elastic tools, cavity forming processes (pneumatic bulging) of superplastic sheet metal forming, laser forming and laser assisted forming, magnetic-pulse forming, shot peen forming and methods of incremental forming.

Sheet hydroforming (SHF) is a technology that uses hydraulic fluid taken to very high pressure as an essential tool in transforming sheet metal and tubes fitted to a specially designed die. Sheet hydroforming technology is classified into SHF with a punch (SHF-P) and SHF with a die (SHF-D) depending on whether a punch or a die will be used to form the blank. In hydroforming processes there is a possibility to make complex metal parts, with special curves, even with unusual shapes and a possibility to reduce the number of components in a product, resulting in economic savings and increased performance. Nowadays, SHF is widely accepted for the industrial produced components characterized by fine surface quality, accurate dimensions, high drawing ratios, and complex shapes [28]. Multi-stage SHF increases the formability of structural parts [29]. SHF technologies are now commonly used in automotive industries to produce fuel tanks and tubular parts for exhaust systems. The last technological development in hydroforming techniques consists of combining tube bending, tube hydroforming and tube welding in a flexible manner using reconfigurable machine tool equipments easily adaptable to various production batches [30]. Flexforming is a type of hydroforming process in which the sheet metal is forced to take the shape of a rigid die by the action of fluid pressure which acts through a rubber diaphragm (Fig. 4). In this process there is only a single rigid die providing low die costs, the easy modification of the dies after changes leading to fast tryouts, and finally high quality parts. The flexforming process needs

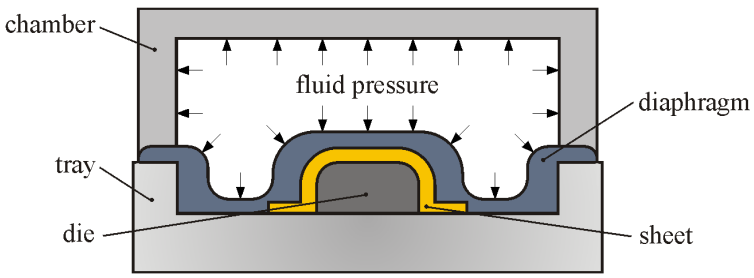

Fig. 4. The schematic representation of the flexforming process

special presses to stand for high pressures up to 80 MPa in the pressure chamber. Sheet metal forming with elastic tools is commonly used in aircraft industry, especially for forming stainless steels nickel alloys sheets.

In order to reduce setup time of production and production cost in small batch production the incremental forming (IF) may be used. IF is dieless forming process and has demonstrated its great potential to form complex three-dimensional parts with using a relatively simple and low cost tools. The theory is that delaminating a complex surface 3D digital model along the contour line, and forming a series of section 2D data, the doing plastic forming from the top to the bottom level by level and part by part according to the section 2D data. Negative dieless incremental forming, also known as single point incremental forming (SPIF) is the earliest form of incremental forming. Positive die-less incremental forming is also referred to as two point incremental sheet forming (TPIF). The main advantages of incremental forming are high process flexibility, relatively low hardware costs and enhanced formability (Fig. 5) [31, 32]. A greater deformation of a sheet metal can be achieved in the incremental forming compared to conventional forming [33]. The forming limit curve, which depicts the formability in the major and minor strain space, is expressed as a straight line with a negative slope. It is noted [33] that formability is the greatest under plane-strain stretching, during which the minor strain is zero. Potential application areas of IF include aerospace industry, biomedical applications and prototyping in the automotive industry.

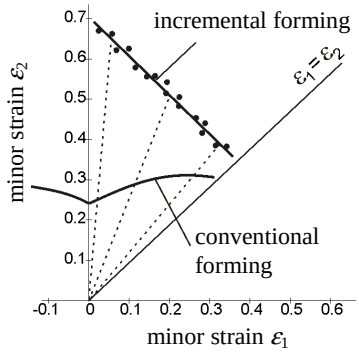

Fig. 5. Forming limit curve in IF compared to conventional forming limit curve: material with good formability (aluminium)

One variant of SPIF method is forming by water jet [34] as a forming tool, where the metallic contact between forming tools and the sheet was eliminated. This new variant such as the water jet system is a force controlled operation whereas the numerically controlled tool system used in SPIF is a displacement controlled system. Water jet forming is a special variant of incremental forming, where a high-pressure water jet has replaced the common steel punch. In water jet forming process a can is placed inside a mould (die) and over a set of rotating

nozzles – typically 2 (Fig. 6). The rotating nozzles produce columnated (straight) high pressure water jets that spray against the can wall and push the can wall outwards. At the same time the nozzles move vertically at a constant speed, so that the point of impact of the water jet travels over the can wall in a spiral trajectory [34]. Typical parameters of the water jet forming process are: nozzle rotation 5000 rpm, water pressure 100-350 bar.

To form hard deformable alloy sheets, especially magnesium and titanium alloys, a hot incremental forming (HIF) has been developed [35]. Possibility to realize IF in conventional CNC controlled machine causes that there is not observed a significant progress in production of specialized CNC machines for incremental forming. The exceptions are machines of AMINO Corp. series DLNC with movable table and with feeding speed up to 60 m/min allowing to form e.g., aluminium alloy sheets with thickness 0.5-5 mm and stainless steel sheets with thickness up to 2 mm [6].

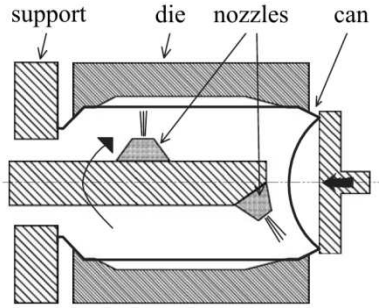

Fig. 6. Scheme of water jet forming process, prepared on the basis of [34]

The electromagnetic forming process (EMF) is a highly dynamic process using pulsed magnetic fields to form metals with high electrical conductivity such as aluminium. In this process, deformation of the workpiece is driven by the interaction of a current generated in the workpiece with a magnetic field generated by a coil adjacent to it. Due to the process principle local workpiece velocities of more than 300 m/s [36] are achievable within the EMF process, whereby a high contact force between the workpiece and the die occurs during the impact. The EMF technique is particularly attractive for the aerospace and automotive industries due to several potential advantages over conventional forming methods: low-cost single-side tooling, high speed (typical EMF current pulse rise times are on the order of 20 μs and after electromagnetic launch deformation may persist for a time on the order of milliseconds) and precise process control [37]. Compared with other sheet metal forming techniques, EMF offers several advantages [38]. However, there are also a number of limitations [38]:

- only relatively thin-walled workpieces can be electromagnetically formed,
- EMF does not lend itself to processes such as deep drawing where significant material must be drawn in over the edges of the die with the aid of lubricants,
- only highly conductive workpieces or workpieces with highly conductive driver plates can be formed using this method.

Typical system for EMF process has been shown in Fig. 7.

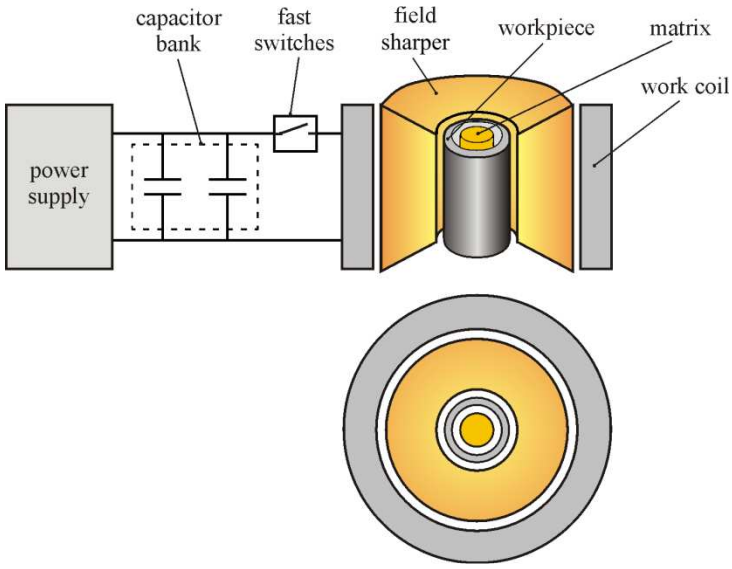

Fig. 7. EMF system with field shaper for compressing cylindrical

5. Conclusion

The development of computer numerical control machines for metal forming is directed on improvement of part quality, increase of productivity with concomitant performed economical and environmental protection aspects. In the metal forming machines area the development progression in automatic tool change system and part manipulation is evident. The technological progress is connected with introducing into the market self-service machines and autonomic modular machine production lines. With the CNC machines for metal forming simultaneously the development of systems for simulation of metal forming processes based on computer modelling is observed. Modern metal forming machine tools must conform to the current level of automated production, therefore they are equipped in monitoring and diagnostic system. Control systems of

metal forming parameters are equipped in intelligent functions enable to on-line processing. Two main progress directions should be taken into consideration at further development of sheet metal forming technology. Firstly, the costs of development and production of new machines for forming of complex shell parts are extremely high and should be reduced. Secondly, it is necessary to reduce the time for developing, designing and producing the dies for the production of parts.

References

[1] Honczarenko J.: Rozwój i automatyzacja obrabiarek skrawających, cz. II, Mechanik, 83 (2010), 90-94.
[2] Kosmol J.: Kierunki rozwoju obrabiarek. Reminiscencje z Salonu MACH-TOOL na ITM 2011, Mechanik, 84 (2011), 660-664.
[3] Plewiński A.: Kierunki rozwoju maszyn do obróbki plastycznej, Obróbka Plastyczna, 16 (2005), 21-28.
[4] Trzepieciński T.: Rosnące znaczenie obrabiarek CNC w procesach obróbki plastycznej blach, Mechanik, 85 (2012), CD1.
[5] Kosmol J.: Tajwan – lider w produkcji obrabiarek. cz. I, Mechanik, 85 (2012), 26-28.
[6] Materiały firmowe i reklamowe firm: AMINO, SEYI.
[7] Trzepieciński T.: Trendy rozwojowe maszyn i technik stosowanych w technologii cięcia blach, Inżynieria Maszyn, 17 (2012) (accepted for publication).
[8] Hassan M.A., Takakura N., Yamaguchi K.: Friction aided deep drawing using newly developed blank-holder divided into eight segments, Int. J. Machine Tools Manuf., 43 (2003), 637-646.
[9] Ali S., Hinduja S., Atkinson J., Bolt P., Werkhoven R.: The effect of ultra-low frequency pulsations on tearing during deep drawing of cylindrical cups, Int. J. Machine Tools Manuf., 48 (2008), 558-564.
[10] Lim Y., Venugopal R., Ulsoy A.G.: Multi-input multi-output (MIMO) modeling and control for stamping, J. Dyn. Syst. Meas. Contr., 132 (2010), 1-12.
[11] Drenger T., Pawlicki M.: Nowoczesne systemy docisku blachy w procesie tłoczenia, Obróbka Plastyczna, 22 (2011), 83-109.
[12] Wifi A., Mosallam A.: Some aspects of blank-holder force schemes in deep drawing process, J. Achievements Mat. Manuf. Eng., 24 (2007), 315-323.
[13] Mori T., Uchida Y.: Effect of vibration on the blank holder in cup drawing, Proc. of 21st Int. Machine Tool Design and Research Conf., 1990, 237-242.
[14] Wifi A.S., Abdelhamid A.: Finite element analysis of deep drawing using a vibrating blank holder, Advances in Material and Processing Technologies AMPT'07, University of Minho, Portugal 1997, 815-822.
[15] Siegert K., Ziegler M.: Pulsating blankholder force in the deep drawing processes, Annals CIRP, 46 (1997), 205-208.
[16] Thiruvarudchel van S., Lewis W.G.: Deep drawing with blank holder force approximately proportional to the punch force, ASME J. Eng. Ind., 112 (1990), 278-285.
[17] Ragab M.S., Sommer H.: Deep drawing with elastic blankholder (in German), Bänder Bleche Rohre, 25 (1984), 225-258.

[18] Hassan M.A., Takakura N., Yamaguchi K.: Friction aided deep drawing using polyurethane ring and metal punch. Part 1: experimental observations on the deep drawing of aluminum thin sheets and foils, Int. J. Machine Tools Manuf., 42 (2002), 625-631.
[19] Kadkhodayan M., Poursan R.: Finite element simulation of process and springback of friction aided deep drawing using tapered blank holder divided into eight segments, Int. J. Adv. Des. Manuf. Technol., 3 (2010), 1-10.
[20] Hassan M.A., Suenaga R., Takakura N., Yamaguchi K.: A novel process on friction aided deep drawing using tapered blank-holder divided into four segments, J. Mater. Proc. Technol., 159 (2005), 418-425.
[21] Pham D.T., Su S.Z., Li M.Z., Liu C.: Digital dieless tooling and jigless tooling technology for manufacturing 3D panels using multi-point forming methodology, Proc. of Innovative Production Machines and Systems Conf. (IPROMS), 2007, 6-11.
[22] Hardt D.E., Norfleet N.A., Valentin V.M., Parris A.: In-process control of strain in a stretch forming process, J. Mater. Proc. Technol., 123 (2001), 496-503.
[23] Lim Y.S., Venugopal R., Ulsoy A.G.: Multi-input multi-output modeling and control for stamping, J. Dyn. Syst. Meas. Contr., 132 (2010), 1-12.
[24] Wang L., Lee T.C.: Controlled strain path forming process with space variant blank holder force using RSM method, J. Mater. Proc. Technol., 167 (2005), 447-455.
[25] Xu S., Zhao K., Lanker T., Zhang J., Wang C.T.: On improving the accuracy of springback prediction and die compensation, SAE Paper No 2007-01-1687.
[26] Lim Y., Venugopal R., Ulsoy A.G.: Improved part quality in stamping using multi-input multi-output (MIMO) process control, Proc. of American Control Conf., St. Louis 2009, 5570-5575.
[27] Siegert K., Hohnhaus J., Wagner S.: Combination of hydraulic multipoint cushion system and segment-elastic blankholders, Proc. of International Congress & Exposition, Session: Sheet Metal Stamping, Detroit 1998.
[28] Tseng H.C., Hung J.C., Hung C., Lee M.F.: Experimental and numerical analysis of titanium/aluminum clad metal sheets in sheet hydroforming, Int. J. Adv. Manuf. Technol., 54 (2011), 93-111.
[29] Chen W, Liu Z.J., Hou B., Du R.X.: Study on multi-stage sheet metal forming for automobile structure-pieces, J. Mater. Proc. Technol., 187-188 (2007), 113-117.
[30] Chinesta F., Cueto E.: Advances in material forming, Springer-Verlag, Paris 2007.
[31] Attanasio A., Ceretti E., Giardini C., Mazzoni L.: Asymmetric two points incremental forming: Improving surface quality and geometric accuracy by tool path optimization, J. Mater. Proc. Technol., 197 (2008), 59-67.
[32] Trzepieciński T., Kowalik M.: Rozwój metod jednopunktowego tłoczenia przyrostowego na obrabiarkach CNC, Mechanik, 85-1 (2012), CD1.
[33] Kim Y.H., Park J.J.: Effect of process parameters on formability in incremental forming of sheet metal, J. Mater. Proc. Technol., 130-131 (2002), 42-46.
[34] Emmens W.C.: Water jet forming of steel beverage cans, Int. J. Machine Tools Manuf., 46 (2006), 1243-1247.
[35] Fan G., Gao L., Hussain G., Wu Z.: Electric hot incremental forming: A novel technique, Int. J. Machine Tools Manuf., 48 (2008), 1688-1692.

[36] Ungera J., Stiemerb M., Schwarzec M., Svendsena B., Blumb H., Reesec S.: Strategies for 3D simulation of electromagnetic forming processes, J. Mater. Proc. Technol., 199 (2010), 341-362.
[37] Thomas J.D., Seth M., Daehn G.S., Bradley J.R., Triantafyllidis N.: Forming limits for electromagnetically expanded aluminum alloy tubes: Theory and experiment, Acta Materialia, 55 (2007), 2863-2873.
[38] El-Azab A., Garnich M., Kapoor A.: Modeling of the electromagnetic forming of sheet metals: state-of-the-art and future needs, J. Mater. Proc. Technol., 142 (2004), 744-754.

POSTĘPY W TECHNOLOGIACH KSZTAŁTOWANIA BLACH

Streszczenie

W artykule przedstawiono zmiany zachodzące w budowie maszyn stosowanych w technologiach matrycowego i bezmatrycowego kształtowania blach. Wskazano wybrane kierunki rozwoju technologii i maszyn do kształtowania blach, uwzględniając nowoczesne systemy docisku blachy stosowane w tłocznikach. Przedstawiono także tendencje we wprowadzaniu nowych technologii oraz modernizacji obecnie stosowanych celem zwiększania produktywności.

Słowa kluczowe: dociskacz, system docisku, tłoczenie, obróbka blach

DOI: 10.7862/rm.2012.12

RECENZENCI WSPÓŁPRACUJĄCY – 2012 r.

Tadeusz BALAWENDER
Józef BRZĘCZEK
Grzegorz BUDZIK
Emil EVIN
Wiesław FRĄCZ
František GREŠKOVIČ
Marek KOWALIK
Hirpa G. LEMU
Volodymyr LIUBYMOV
Jerzy ŁUNARSKI
Antoni ORŁOWICZ
Zbigniew PATER
Paweł PAWLUS
Valery SHEVELYA
Janusz SIKORA
Leszek SKOCZYLAS
Ján SLOTA
Feliks STACHOWICZ
Tomasz TRZEPIECIŃSKI
Łukasz WĘSIERSKI
Władysław ZIELECKI